St. John's University

St. John's Scholar

2021

ANTICANCER EFFECT OF INDANONE-BASED THIAZOLYL HYDRAZONE DERIVATIVE ON P53 MUTANT COLON CANCER CELL LINES: IN VITRO AND IN VIVO STUDY

Silpa Narayanan

ANTICANCER EFFECT OF INDANONE-BASED THIAZOLYL HYDRAZONE DERIVATIVE ON P53 MUTANT COLON CANCER CELL LINES: *IN VITRO* AND *IN VIVO* STUDY

A dissertation submitted in partial fulfillment
of the requirements for the degree of

DOCTOR OF PHILOSOPHY

to the faculty of

DEPARTMENT OF PHARMACOLOGY

of

COLLEGE OF PHARMACY AND HEALTH SCIENCES

at

ST JOHN'S UNIVERSITY

New York

by

SILPA NARAYANAN

Date submitted_____   Date approved_____

_____   _____

Silpa Narayanan   Dr. Zhe-Sheng Chen

ABSTRACT

ANTICANCER EFFECT OF INDANONE-BASED THIAZOLYL HYDRAZONE DERIVATIVE ON P53 MUTANT COLON CANCER CELL LINES: *IN VITRO* AND *IN VIVO* STUDY

SILPA NARAYANAN

Colorectal cancer is the third leading cause of cancer related deaths in the United States. Currently, irinotecan, a topoisomerase I inhibitor, is an important anticancer drug approved for patients with advanced or recurrent colorectal cancer. Considering the low response rate and the events of high toxicity caused by irinotecan, we evaluated a series of thirteen thiazolyl hydrazone derivatives of 1-indanone for their potential antineoplastic activity and four compounds showed promising anticancer activity against most of the tested colon cancer cell lines with IC_{50} values ranging from 0.41 ± 0.19 to 6.85 ± 1.44 μM. It is noteworthy that the compound, N-Indan-1-ylidene-N'-(4-Biphenyl-4-yl-thiazol-2-yl)-hydrazine (ITH-6) is found to be more effective than irinotecan against p53 mutant colon cancer cells, HT-29, COLO 205, and KM 12 than p53 wild-type colon cancer cell line such as HCT 116. Mechanistic studies reveal that ITH-6 arrests these cancer cell lines in G2/M phase of the cell cycle, induces apoptosis, and causes an increase in ROS level with a significant reduction in the GSH level. The cell cycle arrest is related to the inhibition of tubulin polymerization in the mitotic phase. Moreover, ITH-6 inhibits the expression of NF-kB p65 and Bcl-2, which proves its cytotoxic action. The downregulation of NF-kB p65 can be further proved by immunofluorescence. Moreover, CRISPR/Cas9 was applied to establish NF-kB p65 gene knockout HT-29 cell model to validate the target of ITH-6.

In addition, ITH-6 significantly decreased tumor size, growth rate and tumor volume in mice bearing HT-29 and KM 12 tumor xenografts. Overall, the results suggest that ITH-6 could be a potential anticancer drug candidate for p53 mutant colon cancers.

ACKNOWLEDGEMENTS

TABLE OF CONTENTS

LIST OF TABLES

LIST OF FIGURES

CHAPTER 1. Introduction

Cancer remains the most intriguing disease of human populations in terms of its types, progression and treatment(1–3). Despite of the advances in the field of cancer research and translational medicine, which has indeed resulted in higher cure rates for various tumor types, cancer remains the second leading health challenge, after heart related disorders in both developing and developed countries(4,5). Among malignancies, colorectal cancer (CRC) is the third most commonly diagnosed malignancy and the fourth leading cause of cancer related deaths globally(6). CRC is considered to be an environmental disease, affected by cultural, social and lifestyle practices(7). Studies done in the past have shown that endocrine factors and obesity are the two major contributors to an increase in the risk of CRC(8). Moreover, weight gain during the middle age and metabolic dysfunctions can predispose to abdominal obesity which positively correlates with CRC(9). It has also been found that the dietary habits influence the risk of CRC. The dietary fat especially from animal sources has earlier been demonstrated to be metabolized into a carcinogen by colonic flora(10). Moreover, the genetic makeup of individuals also plays an important role in its genesis and mutations in chromosome 18q have resulted in errors in DNA replication which account for 15–20% of sporadic colon cancer(11,12). According to the American Cancer Society, around 104,610 CRC cases were diagnosed in 2020 in the United States with around 53,200 deaths estimated from the disease(13). Studies have shown that approximately 30% of CRC cases are hereditary in nature(14). The etiology remains unknown for around 75% cases of CRC and the remaining small percentage of cases are due to familial incidences or inflammatory bowel disease. Around 33% of familial cases have a genetic basis(15). Surgery is the primary treatment option for most cases of

CRC(16). The current pharmacological management of primary CRC is based on the drug regimens such as FOLFOX and FOLFIRI for metastatic CRC. Though therapeutically efficacious, these anticancer agents bear several side effects such as nausea, vomiting, diarrhea, neurotoxicity, and infections which frequently reach to the level of causing a halt of the treatment(17,18). Targeted specific drugs such as regorafenib, cetuximab, and bevacizumab have now been approved as alternatives for the treatment of CRC(19,20). Although these drugs are effective and increase the overall survival, the existence of drug resistance mechanisms and toxicity remain serious concerns(21,22). Since previous studies have established that the indanone ring exerts anticancer activity(23–26), here we investigate the anticancer effects of a series of indanone-based thiazolyl hydrazones on different human cancer cell lines.

1.1 Biological activities of indanones and related compounds

Indanones and related compounds are important bioactive molecules. These compounds have been studied for various biological activities including cancer and Alzheimer's type of diseases(27). Indanone and its analogues are being developed to combat drug-resistant malignancies(28). Another indanone analogue, donepezil hydrochloride has been approved by US-FDA for the treatment of mild to moderate Alzheimer's disease. This drug acts as an acetylcholinesterase inhibitor and some other indanones have been isolated from natural products(29). Being such a useful moiety, several synthetic strategies have also been developed for their synthesis. Extensive studies on bioactivity of indanone derivatives open up more and more new possibilities of their applications as antiviral and antibacterial agents(30), anticancer drugs(31), pharmaceuticals used in the Alzheimer's disease treatment(32), cardiovascular drugs(32), insecticides, fungicides, herbicides(33) and non-

nucleoside, low molecular drugs for the hepatitis C treatment, which inhibit HCV replication(34,35). Moreover, the derivatives of indanone are being developed to treat drug-resistant malignancies in some cell lines i.e., KB403 (oral and mouth cancer cells), WRL68 (liver cancer cells), CaCO2 (colon cancer cells), HepG2 (liver cells) and MCF7 (hormone-dependent breast cancer cells)(36).

1.2 Overview of NF-kB signaling pathway

The nuclear factor-kappa B (NF-kB) is a key regulator of inflammation and has been associated with carcinogenesis(37). The NF-kB family is comprised of 5 subunits, RelA (p65), RelB, NF-kB1 (p50 and its precursor p105), NF-kB2 (p52 and its precursor p100), and c-Rel(38). There are two pathways for NF-kB activation, canonical and non-canonical pathway. The canonical activation of the NF-kB signaling pathway by cytokines, such as interleukin-1(IL-1) and tumor necrosis factor (TNF) stimulate the IkB kinase (IKK) complex which causes the degradation of Inhibitor of Kappa Light Chain Gene Enhancer in B Cells, Alpha (IkBα) by ubiquitin proteasome system and release the NF-kB subunits into the nucleus where they become active and induce gene expression. The modulators involved in the canonical pathway are IKKs including IKKα, IKKβ and IKKγ or NEMO. The alternative pathway (non-canonical pathway) includes B-cell activation factor (BAFF-R), lymphotoxin β-receptor (LTβR), and CF40 receptor activator for nuclear factor-kappa B (RANK) which in turn activate adaptor protein NF-kB-inducing kinase (NIK) which activates IKKα(39).

As indicated above, in unstimulated cells, NF-kB dimers are localized in the cytoplasm through their association with IkB proteins. However, it has been reported that the complex constituted by IkBα and the p50/p65 dimer can shuttle between the cytoplasm and the

nucleus, although it remains transcriptionally inactive. Indeed, only after degradation of IkB proteins, this dimer localizes to the nucleus and binds to DNA(40,41). Several IkB proteins have been identified, including IkBα, IkBβ, IkBε, IkBκ, and B-cell lymphoma 3 (Bcl-3) (40,42). IkBα and IkBβ are the best known members of the IkB family, as they are expressed in almost all tissues; conversely, the expression of IkBε, IkBζ, and Bcl-3 is restricted to hematopoietic cells(41,42). The primary target of IkBα is the dimer p50/p65, whereas IkBβ is associated mainly with p65/c-Rel dimers.

It has been reported that NF-kB activation in the intestinal epithelial cells has a key role in tumor formation. NF-kB is a transcription factor which can regulate over 200 genes those are involved in cell survival and inflammation(38). There is strong relation between that inflammation and occurrence of CRC. NF-kB activation has a pro-inflammatory and pro-tumorigenic roles (43).

1.3 Role of NF-kB in cancer

NF-kB signaling is involved in cellular immunity, inflammation, and stress, as well as regulation of cell differentiation, proliferation, and apoptosis(44–48). The NF-kB pathway is often altered in both solid and hematopoietic malignancies, promoting tumor-cell proliferation and survival(49,50). Prolonged chronic inflammation may cause tissue damage, degenerative diseases, and cancers of multiple types by inducing cellular stress, recruiting inflammatory factors, and DNA damage. Moreover, chronic inflammation also results in tumorigenesis by genetic mutations and epigenesis. (51). Inflammation increases the risk of tumor formation by disabling the immune system from attacking tumor cells and by inducing the cell proliferation and genetic instability that leads to oncogenic

mutations. NF-kB is the regulator of inflammation and cancer. In cancerous cells with elevated NF-kB activity, the accumulation of proinflammatory cytokines at the tumor site promotes the pro-tumorigenic microenvironment. In patients with inflammatory bowel disease (IBD), pro-tumorigenic cytokines such as TNF-α, IL-1, and IL-17 elevate NF-kB activity which may increase the risk of colon cancer(52). Chronic inflammation can lead to genomic instability and genetic mutations may favor tumor initiation and development(53,54). At the site of inflammation, reactive oxygen species (ROS) are released by neutrophils and macrophages and cause DNA damage which can activate the NF-kB pathway and form a positive feedback loop to enhance NF-kB activity in different types of cells at the site of inflammation. Furthermore, NF-kB induces the expression of anti-apoptotic genes such as the caspase-8 inhibitor FLIP and members of the B-cell lymphoma 2 (Bcl-2) family of apoptosis regulators. These evidences support the facts that tumor cells may also depend on the NF-kB pathway to escape from apoptosis, which has been identified as one of the essential hallmarks of cancer(51). Based on the results, it is possible that the role of NF-kB in certain types of cancer and at certain stages of cancer development is mainly through promoting cell proliferation rather than inhibiting apoptosis.

1.4 p53 status and NF-kB

Regulation of cellular metabolism by NF-kB depends on the status of tumor suppressor gene, p53, in the cells. This is one of the many aspects of the crucial crosstalk between NF-kB and p53. Many oncogenic mutations, such as those in epidermal growth factor receptor (EGFR), Ras, phosphoinositide 3-kinase (PI3K) and p53, contribute to NF-kB activation in tumor cells. Kras and p53 mutations have been found in 20-25% and in ~50% of all

cancers, respectively, and the mutation rates are especially high in pancreatic, CRC and lung cancers(55). The crosstalk between p53 and NF-kB has drawn much attention in the cancer research community. As described above, wild-type p53 antagonizes NF-kB function and suppresses tumorigenesis; about 50% of human cancers acquire p53 mutations (or lose the wild-type allele) and thus activate the NF-kB pathway during tumor development. The binding of transcription co-factor CBP to p53 or NF-kB decides a cell's fate for apoptosis or survival(56). Furthermore, the NF-kB pathway is also involved in the transcription of mouse double minute 2 (Mdm2), a key ubiquitin E3 ligase of p53, thus indirectly regulating p53 protein stability(57). On the other hand, wild-type p53 may suppress glucose intake and glycolysis by reducing glucose transporter 3 (GLUT3) expression on the cell membrane(58). This may be one of the mechanisms by which wild-type p53 suppresses the NF-kB pathway to a basal level in untransformed cells. In other words, p53 mutations prolong NF-kB activation in the presence of inflammatory stimuli. For example, a recent study examined the correlation between nuclear p65 staining and p53 mutation status in multiple head and neck squamous cell carcinomas and non-small cell lung cancers (NSCLC). They found that mutant p53 overexpression correlates with increased NF-kB activity and reduced apoptosis, while tumors harboring wild-type p53 have much less nuclear p65 staining(59). Furthermore, mice harboring a germline p53 mutation develop more severe chronic inflammation and persistent tissue damage in the dextran sulfate sodium (DSS)-induced mouse colon cancer model. These mice are much more prone to inflammation-associated colon cancer when compared to their p53 wild-type counterparts(59).

Moreover, in this study we explored the mechanisms of action of most active derivative which caused the inhibition of colon cancer cells' proliferation, produced cell cycle arrest, and induced apoptosis, downregulate NF-kB p65 and Bcl-2. The effects of this derivative on tubulin polymerization, production of reactive oxygen species (ROS), glutathione depletion and anticancer activity *in vivo* were also determined.

1.5 NF-kB and Bcl-2

The Bcl-2 family of cell death regulators is critical for determining cell fate in the apoptotic pathway. Bcl-2 and its mammalian homologs Bcl-x_L, Bfl-1 (also called A1), and Mcl-1 block cell death, while Bax, Bcl-x_S, Nbk (also called Bik), Bak, and Bad promote apoptosis(60). Each of these factors influences the cleavage-mediated activation of caspases, which act as the ultimate downstream effectors of the suicide program. Bcl-2-related proteins were shown to block apoptosis in lymphoid cells under conditions in which NF-kB activity was inhibited(61). This raised the possibility that some of these factors may lie downstream of NF-kB in the survival cascade. The pro-survival Bcl-2 homolog Bfl-l is transcriptionally controlled by Rel/NF-kB is consistent with these results(62–65).

Overexpression of members of the Bcl-2 family, such as A1 or Bfl1 and Bcl-xL, inhibit the activation of caspase 9 or proapoptotic Bcl-2 family members produced by inducers of the intrinsic pathway. Inducers of the intrinsic pathway include agents that cause DNA damage or oxidative stress. On the other hand, overexpression of the cellular inhibitors of apoptosis (CIAPs) and Fas-associated death domain-like IL-1β-converting enzyme inhibitor protein (FLIP) modulates the activation of caspase 8 produced by induction of TNF receptor family members. Finally, NF-kB regulates the activation of caspases, including caspases 3 and 7, which result from activation of both apoptotic pathways.

A variety of different NF-kB pathway inhibitors have been developed and are undergoing clinical studies in lymphomas and other malignancies. These include agents that block IKK activity, IkB degradation, NF-kB nuclear targeting, or NF-kB target gene activity(66). The current work provides further understanding of the relative contribution of NF-kB pathway in cancer and its downstream target genes on the activation of each apoptotic pathway, which is important for the design and assessment of novel targeted anticancer agents.

Graphical Abstract: NF-kB pathway in cancer and mechanism of anticancer activity of ITH-6
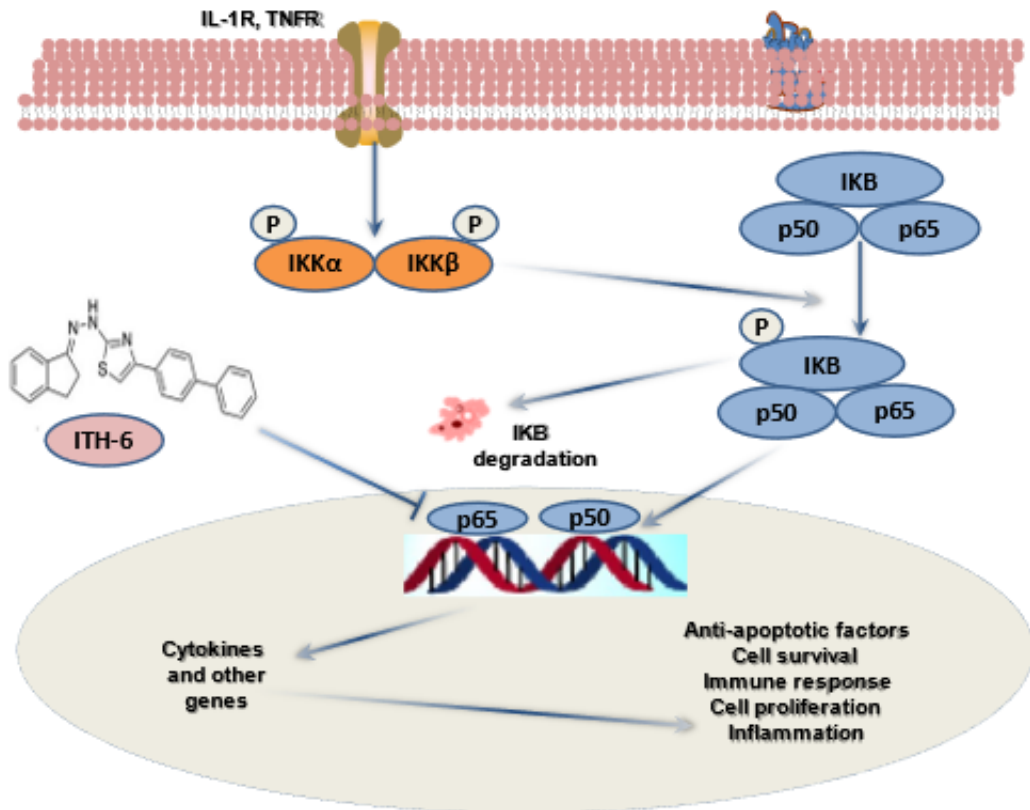
CHAPTER 2. Materials and methods

2.1 Chemicals and equipment

All thiazolyl hydrazone derivatives were synthesized at the University of Karachi, Pakistan (Figure 2). Regorafenib was obtained from Bayer HealthCare Pharmaceuticals Inc. (Whippany, NJ) and irinotecan hydrochloride from Alfa Aesar (Haverhill, MA). Stock solutions (10 mM) of all the compounds in DMSO were prepared and a series of dilutions were made. Figure 3A shows the chemical structure of ITH-**6**. Dulbecco's modified Eagle's Medium (DMEM, IX), fetal bovine serum (FBS), Phosphate Buffer Saline (PBS), 10,000 IU/ml penicillin and 10,000 μg/ml streptomycin, and trypsin 0.25% were purchased from Hyclone (Waltham, MA). 3-(4, 5-dimethylthiazol-2-yl)-2, 5-diphenyl-tetrazolium bromide) (MTT), Dimethyl Sulfoxide (DMSO), and other chemicals were obtained from Sigma-Aldrich Chemical Co (St. Louis, MO). Propidium Iodide (PI)/RNase staining buffer was purchased from BD biosciences (San Jose, CA) and the apoptosis kit were purchased from Biotium (Hayward, CA). 5-(and-6)-chloromethyl-20,7'-dichlorodihydrofluorescein diacetate, acetyl ester (CM-H2DCFDA) was purchased from Molecular probes™ (Eugene, OR). GSH kit from Abcam (Cambridge, MA) and HTS-Tubulin Polymerization Assay Biochem Kit from Cytoskeleton (Denver, CO). Monoclonal antibodies D97JR (selective against ALDH1A1), E7K2Y (against CD44), D14E12 (against NF-kB p65), E4Z1Q (against topoisomerase I), D3R6Y (against procaspase-3), 44D4 (against IkBα) and 16H1 (against GAPDH), D5C9H (against TBP) and secondary anti-rabbit/mouse HRP linked antibody were obtained from Cell Signaling (Danvers, MA). Alexa flour conjugated secondary antibody was obtained from Molecular Probes (Eugene, OR). Trizol reagent was obtained from Invitrogen Life Technologies (Carlsbad, CA). The NF-kB p65, IL-6, Bcl-2

and 18 S TaqMan gene expression kits and superscript IV reverse transcription kit were obtained from Fisher Scientific (Waltham, MA).

2.2 Cell lines and cell culture

HEK293 (human embryonic kidney cell line), NIH/3T3 (mouse fibroblast cell line) and human colon cancer cell lines (COLO 205, HCT-15, SW620, KM 12, HT-29, S1), SNB-19 (human glioblastoma cell line), PC-3 (human prostate cancer cell line), NCI-H460 (human non-small lung cancer cell line), IGROV-1and SK-OV-3 (human ovarian cancer cell lines), ABCB1-overexpressing cancer cell line, SW620/AD300, ABCG2-overexpressing cancer cell line, S1-M1-80 and K-562 (human chronic myeloid leukemia cell line) were used in this study. S1-M1-80 cells were grown in the DMEM medium which has the anticancer drug, mitoxantrone, gradually increasing its concentration up to 80 µg/ml, inducing the overexpression of the ABCG2 transporter(67). SW620/AD300 cells were maintained in complete medium with 300 ng/ml of doxorubicin(68). SW620, SW620/AD300 and S1, S1-M1-80 cell lines were obtained from Dr. Susan E. Bates (Columbia University, New York). All other cell lines were purchased from American Type Culture Collection (ATCC) (Manassas, VA). The cell lines were cultured at 37°C, 5% CO_2 with DMEM containing 10% FBS and 1% penicillin/streptomycin.

2.3 Experimental animals

Male athymic NCR (nu/nu) nude mice (age 5–6 weeks) were purchased from Taconic Farms (Albany, NY) and were used for the animal study. The animals were kept under alternate light/dark cycles, provided with food and water, and kept in polycarbonate cages (4 mice/cage). The mice were housed at the St. John's University Animal Care Center and

were regularly watched for tumor growth by measuring the size using Vernier calipers. The animal protocol was approved by the St. John's University's Institutional Animal Care & Use Committee (IACUC). The research was carried out in compliance with the Animal Welfare Act and the U.S. Health Service.

2.4 Cell proliferation assay

The anticancer effects of ITH-**6,** regorafenib and irinotecan were determined by a 3-(4,5-dimethylthiazol-2-yl)-2, 5-diphenyl-tetrazolium bromide (MTT) calorimetric assay. Cells were cultured, counted, and seeded onto 96 well plates with a cell density of 6×10^3 cells per well. Following 24 h incubation, the cells were treated with different drugs (ranging from a concentration of 0-30 µM). After 68 h, 20 µl of 4 mg/ml MTT, was added to each well and the plates were further incubated 37°C for 4 h. Subsequently, the MTT was removed from all wells and 100 µl of DMSO was added to dissolve the formazan crystals formed by the reduction of MTT in the mitochondria of the viable cells. The optical density (OD) was measured at 570 nm by an Opsys microplate reader (Dynex technologies, VA).

2.5 Cell cycle analysis

Based on the cytotoxic effects of ITH-**6**, the cell cycle analysis was carried out on colon cancer cell lines HT-29, COLO 205, and KM 12. The cells were treated with ITH-**6** at three different concentrations (0.3, 1 and 3 µM) for 24 h and the cell cycle analysis was performed as described previously. In brief, the cells were harvested and centrifuged at 800 rpm for 5 min. The supernatant was removed and the cell pellet was washed with 1X PBS. The cells were fixed overnight in ice cold 70% ethanol at 4°C. The fixed cells were stained with 50 µg/ml PI and 100 µg/ml of RNase at 37°C for 30 min in the dark. The flow

cytometric analysis was performed and the percentage of cells in different phases of cell cycle were determined (G0/G1, S, G2/M).

2.6 Tubulin polymerization assay

The action of the test compound, ITH-**6** on the tubulin polymerization was assessed by tubulin polymerization kit. The preparation of samples and assay protocol was carried out as per manufacturer's instructions. ITH-**6** (100 µM) was used a test compound while paclitaxel and colchicine (10 µM) were used as controls.

2.7 Apoptosis analysis

The cells were incubated with ITH-**6** for 24 h at concentrations of 0.3, 1 and 3 µM. After 24 h, the cells were washed, harvested, and stained with FITC-labeled annexin-V and PI at 37˚C for 30 min. The degree of apoptosis was measured at FL-1 and FL-2 of the flow cytometer.

2.8 Intracellular ROS measurement

In order to investigate the effects of ITH-**6** on the intracellular levels of ROS, the cells were treated with ITH-**6** at different concentrations ranging from 0 to 3 µM for 24 h. After 24 h, the cells were washed and harvested. Subsequently, 10 µM of CM-H2DCFDA was added. The CM-H2DCFDA dye enters into the cells, gets converted into the fluorescent (5-chloromethyl-20-7'-dichlorofluorescein (DCF)) product by the action of intracellular peroxides. The cells were incubated in dark at 37˚C for 30 min. Intracellular ROS levels were measured using the flow cytometer.

2.9 Intracellular GSH assay

In order to better understand the inverse relation between oxidative stress and GSH, the colon cancer cell lines were treated with ITH-**6** at different concentrations 0.3, 1, and 3 µM for 24 h. The intracellular GSH was measured using GSH assay kit and the protocol was carried out as per manufacturer's instructions. The samples were prepared and analyzed as per manufacturer's protocol using FL-1 of flow cytometer.

2.10 Western blot analysis

Western blot analysis was performed to detect the expression level of Aldehyde Dehydrogenase 1 Family Member A1 (ALDH1A1), a cell surface adhesion receptor protein (CD44), a subunit of nuclear factor kappa light chain enhancer of activated B cells (NF-kB p65) (nuclear and cytoplasmic), procaspase-3, topoisomerase I (TOP 1) and IkBα (nuclear and cytoplasmic) proteins after incubating HT-29, COLO 205 and KM 12 cells with different concentrations, 0.3, 1 and 3 µM of ITH-6 for 72 h. Cell lysates were prepared by adding lysis buffer (25 mM Tris-HCl (pH 7.6), 150 mM NaCl, 1% Triton X-100, 1% sodium deoxycholate, 0.1% SDS) to all the three different cell lines. The nuclear and cytoplasmic proteins were separated using NE_PER Nuclear and Cytoplasmic Extraction Reagent Kit (Fisher Scientific). Protein (40 µg) was then resolved by sodium dodecyl sulfate polyacrylamide gel electrophoresis (SDS-PAGE) and transferred onto polyvinylidene fluoride (PVDF) membranes through electrophoresis. Subsequently, PVDF membranes were blocked with 5% non-fat milk dissolved in TBST buffer (10 mmol·L−1 Tris-HCL, 150 mmol·L−1 NaCl and 0.1% Tween20 pH 8.0) for 2 h at room temperature. The samples were incubated with primary antibodies against NF-kB p65 (nuclear and

cytoplasmic), ALDHA1, CD44, IkBα (nuclear and cytoplasmic), procaspase-3, TOP I protein (1:1000) and housekeeping genes, GAPDH and TBP (1:1000) overnight at 4°C and then incubated with peroxidase-conjugated secondary antibodies (1:1000) for 2 h at room temperature. The reaction was visualized by means of enhanced chemiluminescence detection reagents (Amersham, NJ) using the manufacturer's protocol(19). The resulting protein bands were analyzed using Image J software.

2.11 mRNA expression

HT-29, COLO 205 and KM 12 cancer cells were incubated with 0.3, 1 and 3 μM of ITH-6 for 72 h and total RNA was extracted using the RNA extraction trizol reagent as previously described(69). RNA was quantified using Nanodrop and RNA samples with a A260/280 ratio in the range of 1.8 to 2.0 were chosen. These samples were subjected to reverse transcription and the cDNAs formed (by superscript IV reverse transcription kit) were used for quantitative PCR. This analysis was performed using the NF-kB p65, Bcl-2, IL-6 and 18S TaqMan gene expression assay kits. The PCR data were quantitated using the $\Delta\Delta$Ct method and presented as relative - fold of mRNA expression.

2.12 Immunofluorescence

The immunofluorescence assay was performed as previously described(19). Briefly, after being cultured overnight in 24-well plates, cells (2×10^4/well) were treated with ITH-6 (0.3, 1 and 3 μM) for 72 h. Then, cells were fixed in 4% paraformaldehyde for 10 min and permeabilized by 0.1% Triton X-100 for 10 min before being blocked with 6% BSA at 37°C for 1 h. The presence of NF-kB p65 was determined using monoclonal antibody (dilution 1:1000) for incubation at 4°C overnight. Cells were washed with iced PBS after each incubation time. Alexa Fluor 594 (Ex = 561 nm, Em = 617 nm) conjugated secondary

antibody (1:1000) was used after washing with ice cold PBS. DAPI (Ex = 345 nm, Em = 455 nm) was used to counterstain the nuclei. The cells were washed with ice-cold PBS before being imaged. Immunofluorescence images were collected using an EVOS FL Auto fluorescence microscope from Life Technologies Corporation (Gaithersburg, MD).

2.13 Cytotoxicity of ITH-6 on ABCB1 and ABCG2 overexpressing cell lines.

The cytotoxicity assay was conducted in a 96 well plate using parental (SW620 and S1) and drug-resistant (SW620/AD300 and S1-M1-80) cell lines that were seeded at a density of 6×10^3 cells/well. Following 24 h incubation, the cells were treated with ITH-6 (ranging from a concentration of 0-100 μM). After 68 h, the absorbance was measured at 570 nm using spectrophotometer as previously described(70,71) and IC_{50} values were calculated.

2.14 Knockout of NF-kB p65 gene in HT-29 cells

A CRISPR/Cas9 system was used to construct the NF-kB p65 gene knockout subline of HT-29 cells. The custom-designed mammalian CRISPR vector was obtained from Vector Builder Inc. (Chicago, IL). The transfection of the NF-kB p65 targeting vector into HT-29 cells was conducted using Fugene6 transfection reagent (Promega, Madison, WI) according to the manufacturer's instructions. Briefly, HT-29 cells were seeded in 100 mm dishes with 1×10^6 cells per dish and cultured overnight in DMEM with 10% FBS without antibiotics. Then, 10 μg of plasmid DNA was prepared in 376 μl of Opti-MEM medium and mixed with 24 μl of Fugene 6 reagent. Followed by a 30 min incubation at room temperature, the complex was mixed into the cell culture medium and incubated with the cells in a culture incubator for 48 h. At the end of incubation, the transfected cells were rinsed with PBS then incubated with the selection medium containing 2 mg/ml G418 for 3

days. Non-transfected cells were used as negative controls for the selection process. Single colonies of survived cells were obtained and expanded for further study. The knockout of NF-kB p65 was further verified by measuring protein expression using Western blotting and by cell viability study using MTT.

2.15 Molecular modeling

Macintosh Operating System (OS Sierra) with Mac Pro 6-core Intel Xenon E5 processor system was used to perform docking experiments using the Maestro v12. 3. 012 software (Schrödinger, LLC, New York, NY, USA, 2019) software. Lig-prep was used for ITH-6 ligand preparation(72). The heterodimer protein model was imported from the Protein data bank. 'Protein Preparation Wizard' was used for protein preparation. The grid generation was done by selecting residues at 20 Å distance from bound inhibitors in the model protein (1IKN)(73,74). The residues selected were: 26, 28, 29, 30, 49, 50, 181, 222, 224, 225, 236, 237, 238, 239, 241, 258, 259, 260, 261, 275. Extra Precision docking was performed with maximum 10 poses(75).

2.16 Nude mouse MDR xenograft model

The colon cancer cells, HT-29 and KM 12 xenograft mouse models were established as previously reported(76). The cells were implanted subcutaneously into immunocompromised mice under the left and right armpit regions, respectively. When the tumors reached a diameter of around 0.5 cm (day 0) after one week, the mice were randomized into four treatment groups consisting of 6 mice per group as follows: (a) polyethylene glycol 300 as the vehicle which was given orally (q3d × 7), (b) irinotecan (30 mg/kg, q3d × 7) was given intraperitoneally (i.p.), dissolved in normal saline(77) (c) ITH-6 (3 mg/kg) was diluted in PEG 300 and given orally (q3d × 7), and (d) ITH-6 (6 mg/kg)

group was diluted in PEG 300 and given orally (q3d × 7). The treatment was given for twenty-one days and the body weights were recorded every third day to calculate the drug dosage. Tumor volumes (calculated using the two diameters of tumors, termed A and B) were calculated every third day using vernier calipers and calculated using the following formula, $V=\pi/6(A+B/2)^3$ (78,79). The blood was taken via submandibular puncture on the last treatment day and white blood cells (WBC) and platelets counts were determined in all four groups.

At the end of the treatment regimen, the mice were euthanized, and the tumors were removed and weighed.

2.17 Collection of plasma and tumor tissues

In separate experiments, mice bearing HT-29 and KM 12 tumors were separated into three groups: (i) mice receiving 3 mg/kg ITH-6 orally (ii) 6 mg/kg ITH-6 orally and (iii) 30 mg/kg i.p. irinotecan. Animals were anesthetized with 3 % isoflurane and 50 μL of blood was collected 5, 30, 60, 120,180 and 240 min after the appropriate treatment, by submandibular puncture into heparinized tubes. In addition, the tumors were excised, weighed, and stored at - 80°C for further study.

2.18 HPLC protocol for plasma sample collection

To the collected plasma samples 500 ml methanol: TFA (10:1) mixture was added and it was incubated on ice for 30 min to allow protein precipitation. It was then centrifuged at 15000 rpm at 4º C for 20 min. The supernatant was collected and filtered through 0.2 mm filter into HPLC vials and then the samples were analyzed using HPLC.

2.19 HPLC protocol for tumor sample collection

The tumors were homogenized in 10 ml PBS. The homogenized mixture was extracted using 10 ml diethyl ether. The mixture was centrifuged at 4° C at 1,500 rpm for 10 min and then the diethyl ether layer was collected. The solvent was evaporated, and the residue was redissolved in 500 ml methanol: TFA (10:1) mixture. It was incubated on ice for 30 min to allow protein precipitation. It was then centrifuged at 15,000 rpm at 4°C for 20 min. The supernatant was collected and filtered through 0.2 mm filter into HPLC vials and then the samples were analyzed using HPLC.

2.20 HPLC method.

The Agilent 1260 infinity series was used to analyze the samples. The ACE C18 column with dimensions 5 mm x 250 x 4.6 mm was used. The solvent system used was A= water (with 0.1% formic acid) and B= methanol (with 0.1% formic acid). The injection volume used was 100 µl and the detector wavelength used was 254 nm.

Method for Irinotecan: Flow rate: 0.5 ml/min

Time (min)	Solvent A percentage	Solvent B percentage
0	60	40
10	98	2
12	98	2
15	60	40

Method for ITH-6: Flow rate: 0.5 ml/min

Time (min)	Solvent A percentage	Solvent B percentage
0	60	40
20	98	2
22	98	2
25	60	40

The t_R (retention time) for irinotecan was 6.2 min and t_R for ITH-6 was 17.5 min.

The standard curve was created based on dosage. Irinotecan (2 mg/ml, 1mg/ml, 0.5 mg/ml, 0.25 mg/ml, 0.125 mg/ml, 0.625 mg/ml) and ITH-6 (1mg/ml, 0.5 mg/ml, 0.25 mg/ml, 0.125 mg/ml, 0.625 mg/ml, 0.313 mg/ml).

2.21 Statistical analysis

All experiments were repeated at least three times and the differences were determined using a one-way analysis of variance (ANOVA). The statistical significance was determined at $p < 0.05$. The post hoc analysis was performed using Tukey's test. The data were analyzed using GraphPad Prism, version 6.

CHAPTER 3. Results

3.1 Non-cytotoxic effect of ITH-6 on normal cell lines.

To determine the cytotoxic effect of ITH-6 on normal healthy cell lines, MTT was carried against human embryonic kidney cell line, HEK293 and mouse fibroblast cell, NIH/3T3. ITH-6 did not show any cytotoxicity on these cell lines and IC_{50} values were more than 30 μM (Table 1).

3.2 ITH-6 inhibits cell proliferation in colon cancer cell lines

In order to determine the cytotoxicity of synthesized compounds on colon cancer cell lines, MTT assay was performed against different cancer cell lines (as mentioned in cell lines and cell culture). The IC_{50} values were >10 μM against all cancer cell lines other than colon cancer cell lines (Table 2). Among all compounds, four compounds exhibited remarkable cytotoxic activities against most of the tested colon cell lines (Table 3). For the five types of tested human colorectal adenocarcinoma cells, SW620, COLO 205, KM 12 and HT-29 cells, ITH-**1** had cytotoxic effects, with IC_{50} values of >10 μM, 1.37 μM, 2.50 μM, and 0.86 μM, respectively. Also, ITH-**3** had cytotoxicity on the same colon cancer cell lines with IC_{50} value of >10 μM, 2.64 μM, 2.91 μM, and 1.99 μM, respectively. The IC_{50} of ITH-6 on HT-29, COLO 205, and KM 12 cell lines (Figure 3B) were 0.40, 0.98 and 0.41 μM, respectively. The IC_{50} was more than 10 μM on HCT-15 cell line. For ITH-**12,** IC_{50} of 2.14 μM on COLO 205, 2.90 μM on KM 12 and 1.17 μM on HT-29 cells were exhibited. IC_{50} values of regorafenib on HT-29, COLO 205 and KM 12 were 22.7 μM, 9.43 μM and 5.02 μM, respectively (Figure 3C). Irinotecan has IC_{50} values of 8.49 μM, 22.84 μM and 23.15 μM on HT-29, COLO 205, and KM 12 cells (Figure 3D). These results indicate that ITH-**6** has a significant effect on the cell viability

of HT-29, COLO 205 and KM 12 cells compared to the other cell lines, suggesting that the drug is more potent to p53 mutant colon cancer cells and chosen for the detailed study of its possible mechanism.

3.3 ITH-6 arrests the colon cancer cells in the G2/M phase of the cell cycle.

In order to investigate the mechanisms by which ITH-**6** inhibits the proliferation of colon cancer cells, its effects on the progression of cell cycle were studied. On treatment with ITH-**6** (0.3, 1, and 3 μM), a concentration dependent increase in the percentage of cells in G2/M phase of the cell cycle of all the three cell lines was observed. The concentrations were selected based on the IC_{50} values. ITH-**6** increased the percentage of cells from 37.5% to 72.1% in HT-29 (Figure 4A), 15.1% to 33.4% in COLO 205 (Figure 4B), and 24.1% to 77.8% in KM 12 cells (Figure 4C). These results suggest that ITH-**6** arrests the cells in G2/M phase with negligible effect on other phases of cell cycle in all the three cell lines.

3.4 ITH-6 inhibits tubulin polymerization in the mitotic phase

To further elucidate the mechanisms by which ITH-**6** arrests the colon cancer cells in G2/M phase of the cell cycle, tubulin polymerization assay was performed according to the manufacturer's protocol. The test drug (ITH-**6**) was compared against control drugs, paclitaxel, and colchicine. Our results indicated that paclitaxel (10 μM) stabilizes the microtubule by enhancing the tubulin polymerization for a period of 1 h while colchicine (10 μM) acted as a tubulin polymerization inhibitor. Interestingly, ITH-**6** at 100 μM inhibited the tubulin polymerization, thus suggesting that ITH-**6** acted on the G2/M phase of the cell cycle by inhibiting the tubulin polymerization activity, an effect like colchicine, however, less potent than colchicine (Figure 5).

3.5 ITH-6 induces apoptosis in colon cancer cells

To understand the apoptotic effects of ITH-**6** on colon cancer cell lines, the cells were treated at different concentrations (0.3, 1, and 3 µM) of ITH-**6** for 24 h. In all the three cell lines, most of the cells were viable in the control group and no apoptosis was observed. ITH-**6** exhibited a concentration dependent increase in the early and late apoptosis of HT-29 (Figure 6A), COLO 205 (Figure 6B), and KM 12 (Figure 6C) cells.

3.6 ITH-6 elevates ROS production in colon cancer cells

Since an increase in intracellular ROS is a measure of induction in apoptosis, we investigated the effects of ITH-**6** on the intracellular ROS production. The cells were treated at the indicated concentrations for 24 h and the intracellular ROS levels were measured using the flow cytometer. As shown in the Figure 7A, ROS percentage increased from 5.98% (control) to 66.30% (ITH-**6** at 3 µM) in HT-29, 1.88% (control) to 71.70% (ITH-**6** at 3 µM) in COLO 205 (Figure 7B), and 4.26% (control) to 69.57% (ITH-**6** at 3 µM) in KM 12 (Figure 7C) cells. These results suggested that ITH-**6** elevates intracellular ROS levels and causes apoptosis in colon cancer cells.

3.7 ITH-6 inhibits GSH levels in colon cancer cells

Since a decrease in GSH levels is known to induce ROS and in turn induce apoptosis, the effects of ITH- **6** on the intracellular GSH levels were determined at the indicated concentrations. Our results showed that ITH-**6** exhibited a concentration-dependent decrease in intracellular GSH levels. As shown in Figure 8A, the GSH percentage decreased from 93.80% (control) to 23.70% (ITH-**6** at 3 µM) in HT-29, from 96.80%

(control) to 34.90% (ITH-**6** at 3 μM) in COLO 205 (Figure 8B), and from 91.30% (control) to 7.81% (ITH-**6** at 3 μM) in KM 12 cells (Figure 8C).

3.8 The effect of ITH-6 on the expression level of different targets associated with apoptosis of colon cancer cells.

To figure out the mechanism of the cytotoxicity of the test compound ITH-6, we performed the Western blotting experiment on various proteins. The proteins selected were ALDH1A1, CD44, NF-kB p65 (nuclear and cytoplasmic), procaspase-3, TOP 1 and IkBα (nuclear and cytoplasm) as they are important prognostic markers in colon cancer cells. HT-29, COLO 205 and KM 12 cells were incubated with 0.3, 1 and 3 μM of ITH-6 for 72 h. At a concentration of 3 μM, ITH-6 downregulated the nuclear NF-kB p65 expression in HT-29 (Figure 10A and C) and COLO 205 (Figure 11A and C) cells compared to the control whereas in KM 12 cells, the test compound at concentrations of 0.3, 1 and 3 μM significantly decreased the nuclear NF-kB p65 expression level compared to the positive control, resveratrol (20 μM) and KM 12 cells are more sensitive to NF-kB p65 downregulation following the treatment with ITH 6 (Figure 12A and C). There was no change in the cytoplasmic NF-kB p65 protein expression in all cell lines treated with ITH-6 (Figure 10, 11 and 12B, D).

Moreover, there was no change in the expression of ALDH1A1 and CD44 (Figure 9), TOP 1 (Figure 13, 14 and 15 C and E) and IkBα (cytoplasmic) levels (Figure 13, 14 and 15 B and D). There was a concentration-dependent decrease in the procaspase-3 expression in COLO 205 and KM 12 (Figure 14 and 15C and F) cells treated with ITH-6 at 3 different concentrations, 0.3, 1 and 3 μM for 72 h whereas in HT-29, there was no change in the expression of procaspase-3 after incubating with ITH-6 (Figure 13C and F). Hence, we can

summarize that the possible mechanism behind ITH-6 induced cytotoxicity in these colon cancer cells results from downregulating nuclear NF-kB p65 protein expression.

3.9 The effect of ITH-6 on the mRNA level of NF-kB p65, IL-6 and Bcl-2 in colon cancer cell lines.

The incubation of HT-29, COLO 205, and KM 12 cancer cell lines with 0.3, 1 and 3 μM of ITH-6 for 72 h remarkably decreased the NF-kB p65 protein expression compared to cells incubated with vehicle. Furthermore, quantitative real-time PCR (RT-PCR) experiments demonstrated that the treatment of these cells with the ITH-6 for 72 h remarkably decreased NF-kB p65 mRNA expression (Figure 16A, B and C).

It was previously indicated that NF-kB p65 transcriptionally regulates IL-6 and Bcl-2, anti-apoptotic proteins(80). Hence, RT-PCR was performed to evaluate the effect of ITH-6 on IL-6 (Figure 17A, B and C) and Bcl-2 (Figure 18A, B and C) mRNA levels and showed that treatment with ITH-6 downregulated the Bcl-2 expression thereby further proving the role of ITH-6 on the apoptosis of these colon cancer cell lines.

3.10 Immunofluorescence

Immunofluorescence experiment was conducted to find out if ITH-6 can downregulate the expression of nuclear NF-kB p65 in HT-29 (Figure 19), COLO 205 (Figure 20), and KM 12 (Figure 21) cells when they are treated with ITH-6 for a period of 72 h. Our results indicated that incubating these colon cancer cells with ITH-6 decreased NF-kB p65 expression which is consistent with the Western blot and RT-PCR results.

3.11 Interaction analysis of ITH-6-NF-kB p65 docked complex

The previously reported IkBα/NF-kB crystal model (PDB code: 1IKN) was used for docking analysis. Stimulation between ITH-6 and the heterodimer complex was performed using induced fit docking. The docking position of ITH-6 showed XP docking score of -5.7 kcal mol^{-1}, which shows good binding affinity. Figure 22A depicts the docking pose and interaction between ITH-6 and the IkBα/NF-kB heterodimer protein. Figure 22B shows H- bonding between the thiazolidine hydrogen and the carbonyl oxygen of GLY259. The biphenyl ring resides in the pocked formed by amino acids: GLN 26, LYS 28, GLN 29, ARG 30, whereas the indene ring sits in the pocked made by amino acids: ARG 236, GLY 237, SER 238, PHE 239, GLN 241.

3.12 ITH-6 is not susceptible to ABCB1- and ABCG2-mediated drug resistance

An MTT assay was performed to examine the susceptibility of ITH-6 to MDR mediated by ABCB1 and ABCG2 transporters. Herein, resistance fold (RF) was used to evaluate if there is any degree of change in the resistance to ITH-6 resulting from the presence of ABCB1 or ABCG2. Based on the results, there was no significant difference in the IC$_{50}$ values of ITH-6 in the ABCB1 overexpressing SW620/AD300 cell line (Figure 23A) and ABCG2 overexpressing S1-M1-80 cell line (Figure 23B) relative to their corresponding parental cell lines.

3.13 Knockout of NF-kB p65 gene in HT-29 cells

The knockout of NF-kB p65 gene in HT-29-NF-kB p65ko cells was verified by the NF-kB p65 protein expression using Western blotting (Figure 24A). The expression level of NF-kB p65 in HT-29-NF-kB p65ko cells was remarkably low compared to that of HT-29 cells (Figure 24B).

To further verify the change in gene expression by targeting NF-kB p65 using the CRISPR/Cas9 system in HT-29-NF-kB p65ko cells, MTT assay was performed. Resistance fold (RF) was used to evaluate if there is any degree of change in the IC_{50} values resulting from the absence of NF-KB p65 expression. Based on the results, the IC_{50} value in HT-29-NF-kB p65ko cells is around 180-fold higher than that of the corresponding HT-29 cell lines (Figure 24C).

3.14 The effect of ITH-6 and irinotecan in mice with HT-29 and KM 12 tumor xenografts

The colon cancer cell lines, HT-29 and KM 12 were implanted subcutaneously and over a period of 7 to 10 days, the mice developed visible tumors and subsequently, the treatment regimen was started. The mice implanted with HT-29 and KM 12 cells had a significant reduction in volume (Figure 24 and 25B) and weight (Figure 24 and 25C) of the tumor after treatment with an oral dose of ITH-6 6 mg/kg compared to the positive control, 30 mg/kg irinotecan which was given intraperitoneally (Figure 24 and 25A). Importantly, the doses that we administered suggested that the treatment did not produce significant overt toxicity as there was no mortality or a significant decrease in body weight (Figure 26A) and no significant change in blood cell count (Figure. 26B and C).

3.15 Concentration of ITH-6 and irinotecan in the tumor and plasma

The plasma level of irinotecan (intraperitoneally) was gradually decreasing as time increases (Figure 27B) and for ITH-6 (given orally), plasma concentration was gradually increasing and reached a peak at 60 min and then decreased (Figure 27A). However, the tumor concentration of irinotecan (30 mg/kg) was less compared to ITH-6 (6 mg/kg) (Figure 28).

Table 1. The effect of ITH-6 on normal cell lines

Compound	HEK 293	NIH/3T3
	IC_{50} (µM)	
ITH-6	>30	>30

µM-Micromole.

The cytotoxic effects of the test compounds on HEK293 (human embryonic kidney cells) and NIH/3T3 (mouse fibroblast cells).

Values in Table 1 are representative of at least three independent experiments performed in triplicates.

IC_{50}: concentration that inhibits cell survival by 50% (mean ± SD).

Table 2: The effect of synthesized compounds on different cancer cell lines.

CELL LINES							
Compounds	**Code**	**SNB-19**	**PC-3**	**NCI-H460**	**IGRO V-1**	**SK-OV-3**	**K-562**
		IC$_{50}$ (µM)					
N-Indan-1-ylidene-*N'*-[4-(4-methoxy-phenyl)-thiazol-2-yl]-hydrazine	ITH-**1**	> 10	> 10	> 10	> 10	> 10	> 10
N-Indan-1-ylidene-*N'*-[4-(3, 5-Dichloro-phenyl)-thiazol-2-yl]-hydrazine	ITH-**2**	> 10	> 10	> 10	> 10	> 10	> 10
N-Indan-1-ylidene-*N'*-[4-(4-Bromo-phenyl)-thiazol-2-yl]-hydrazine	ITH-**3**	> 10	> 10	> 10	> 10	> 10	> 10
N-Indan-1-ylidene-*N'*-[4-(4-Chloro-phenyl)-thiazol-2-yl]-hydrazine	ITH-**4**	> 10	> 10	> 10	> 10	> 10	> 10
N-Indan-1-ylidene-*N'*-[4-(3-nitro-phenyl)-thiazol-2-yl]-hydrazine	ITH-**5**	> 10	> 10	> 10	> 10	> 10	> 10
N-Indan-1-ylidene-*N′*-(4-Biphenyl-4-yl-thiazol-2-yl)-hydrazine	ITH-**6**	> 10	> 10	> 10	> 10	> 10	> 10
N-Indan-1-ylidene-*N'*-(4-phenyl-thiazol-2-yl)-hydrazine	ITH-**7**	> 10	> 10	> 10	> 10	> 10	> 10
N-Indan-1-ylidene-*N'*-[4-(3-Bromo-phenyl)-thiazol-2-yl]-hydrazine	ITH-**8**	> 10	> 10	> 10	> 10	> 10	> 10
N-Indan-1-ylidene-*N'*-[4-(4-nitro-phenyl thiazol-2-yl]-hydrazine	ITH-**9**	> 10	> 10	> 10	> 10	> 10	> 10
N-Indan-1-ylidene-*N'*-[4-(2-hydroxy-phenyl)-thiazol-2-yl]-hydrazine	ITH-**10**	> 10	> 10	> 10	> 10	> 10	> 10
N-Indan-1-ylidene-*N'*-[4-(2,4-Dichloro-phenyl)-thiazol-2-yl]-hydrazine	ITH-**11**	> 10	> 10	> 10	> 10	> 10	> 10
N-Indan-1-ylidene-*N'*-[4-(4-methyl-phenyl)-thiazol-2-yl]-hydrazine	ITH-**12**	> 10	> 10	> 10	> 10	> 10	> 10
N-Indan-1-ylidene-N'-[4-(3-Fluoro-phenyl)-thiazol-2-yl]-hydrazine	ITH-**13**	> 10	> 10	> 10	> 10	> 10	> 10

µM-Micromole

IC$_{50}$: concentration of the drug that inhibits cell survival by 50%

The cytotoxic effects of test compounds on SNB-19 (human glioblastoma cell line), PC-3 (human prostate cancer cell line), NCI-H460 (human lung cancer cell line), IGROV-1 (human ovarian cancer cell line), SK-OV-3 (human ovarian cancer cell line), and K-562 (human chronic myeloid leukemia cell line).

Values in Table 2 are representative of at least three independent experiments performed in triplicates.

Table 3: The effect of synthesized compounds on colon cancer cell lines.

Compounds Code	CELL LINES					
	HCT 116	COLO 205	HCT-15	SW620	KM 12	HT-29
	IC$_{50}$ (µM)					
ITH-**1**	5.04±1.06	1.37±0.29	>10	>10	2.50±0.30	0.86±0.17
ITH-**2**	>10	>10	>10	>10	>10	>10
ITH-**3**	1.25±0.02	2.64±0.35	>10	>10	2.91±0.17	1.99±0.29
ITH-**4**	>10	>10	>10	>10	>10	>10
ITH-**5**	>10	>10	>10	>10	>10	>10
ITH-**6**	5.04±0.20	0.98±0.06	>10	6.85±1.44	0.41±0.19	0.44±0.06
ITH-**7**	>10	>10	>10	>10	>10	>10
ITH-**8**	>10	>10	>10	>10	>10	>10
ITH-**9**	>10	>10	>10	>10	>10	>10
ITH-**10**	>10	>10	>10	>10	>10	>10
ITH-**11**	>10	>10	>10	>10	>10	>10
ITH-**12**	>10	2.14±0.36	>10	>10	2.90±0.06	1.17±0.27
ITH-**13**	>10	>10	>10	>10	>10	>10

µM-Micromole

IC$_{50}$: concentration of drug that inhibits cell survival by 50% (mean ± SD).

The cytotoxic effects of the test compounds on HCT 116, COLO 205, HCT-15, SW620, KM 12, and HT-29 (human colon cancer cell lines).

Values in Table 3 are representative of at least three independent experiments performed in triplicates.
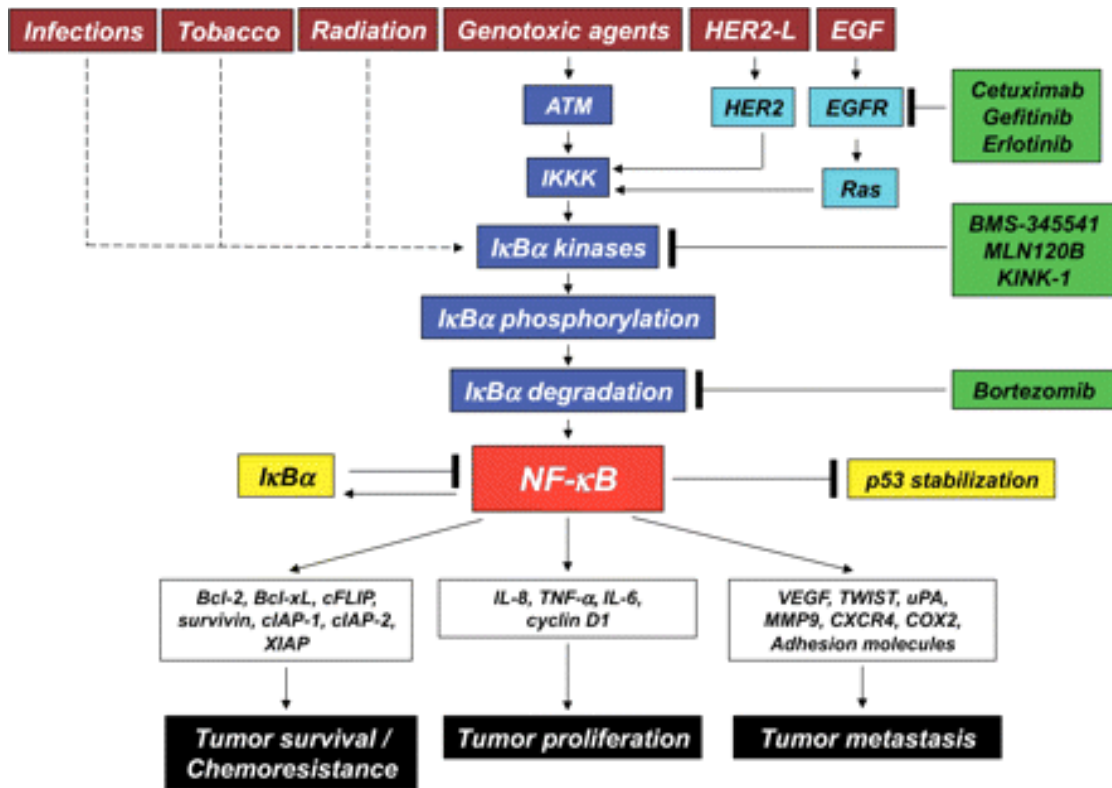
Figure 1 NF-kb pathway

(Adapted from NF-kB in Cancer: A Matter of Life and Death. Aggarwal and Sung. Cancer Discovery, 2011).
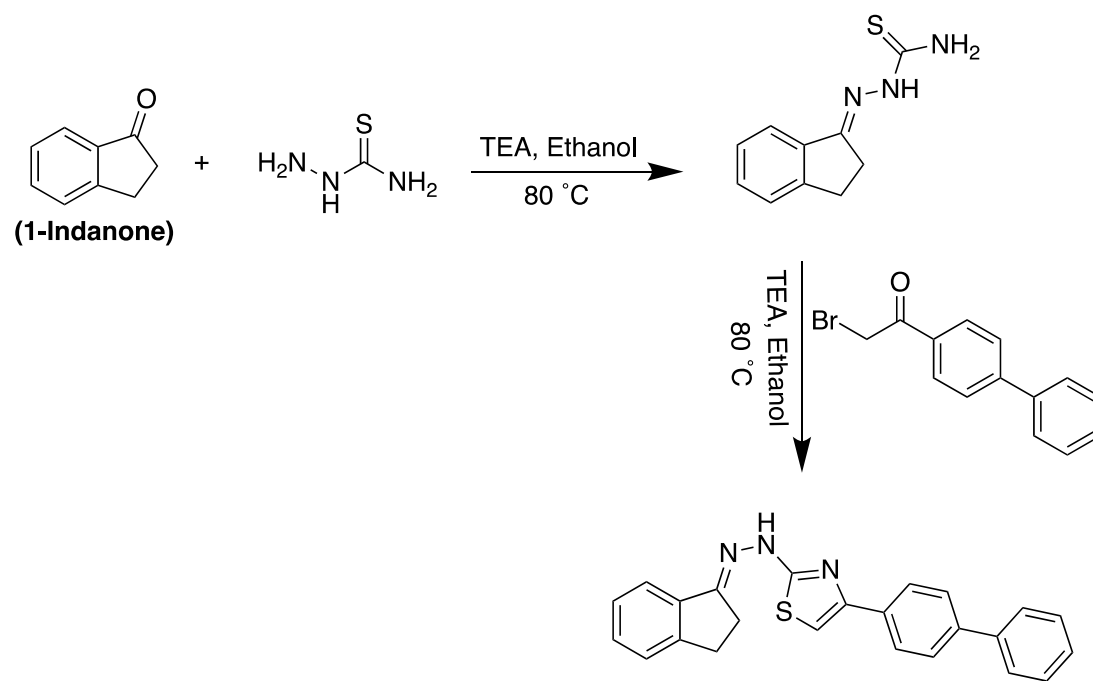
Figure 2

Figure 2. The schematic representation of ITH-6 synthesis from the parent compound, 1-indanone.

Figure 3
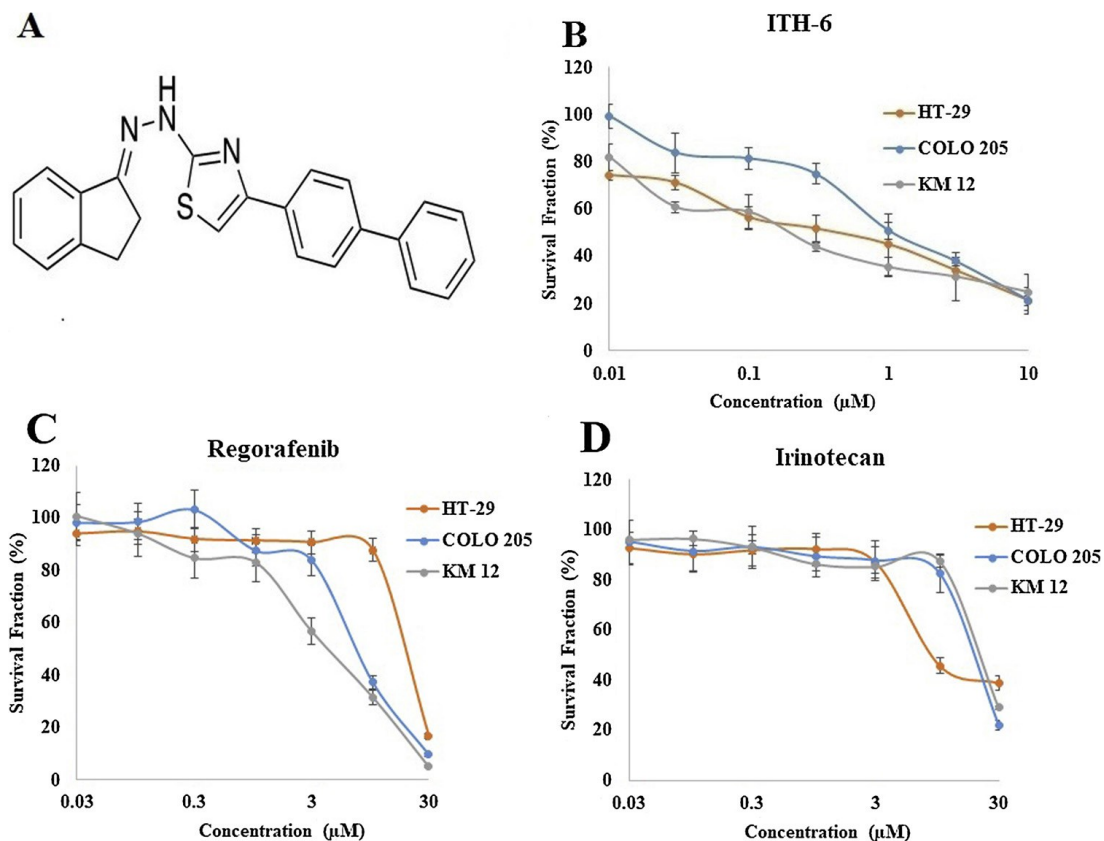
Figure 3. Chemical structure of N-Indan-1-ylidene-N'-(4-Biphenyl-4-yl-thiazol-2-yl)-hydrazine (ITH-6) and cytotoxicity of ITH-6, Regorafenib and Irinotecan in HT-29, COLO 205, and KM 12 cell lines. (A) The chemical structure of ITH-6 was drawn using Chem Draw. Survival fraction (%) was measured after treatment with **(B)** ITH-6, **(C)** Regorafenib and **(D)** Irinotecan for 72 h in HT-29 (orange), COLO 205 (blue), and KM 12 (grey) cell lines. Points with error bars represent the mean ± SD for independent determinations in triplicates. The figure 3B, 3C and 3D are representative of three independent experiments.

Figure 4

Figure 4. Effect of ITH-6 on the cell cycle of HT-29, COLO 205, and KM 12 cell lines. (A) HT-29, **(B)** COLO 205, and **(C)** KM 12 cells were treated with ITH-6 (24 h) in a concentration-dependent manner, stained with propidium iodide (PI), and analyzed by flow cytometer. Quantification of the PI staining data is presented as the percentage of distribution through stages of the cell cycle: blue-G0/G1; red- S; green- G2/M. Points with error bars represent the mean ± SD for independent determinations in triplicates. The figures are representative of three independent experiments. * $p < 0.05$, ** $p < 0.01$, *** $p < 0.001$, and **** $p < 0.0001$ compared to the control group.

Figure 5
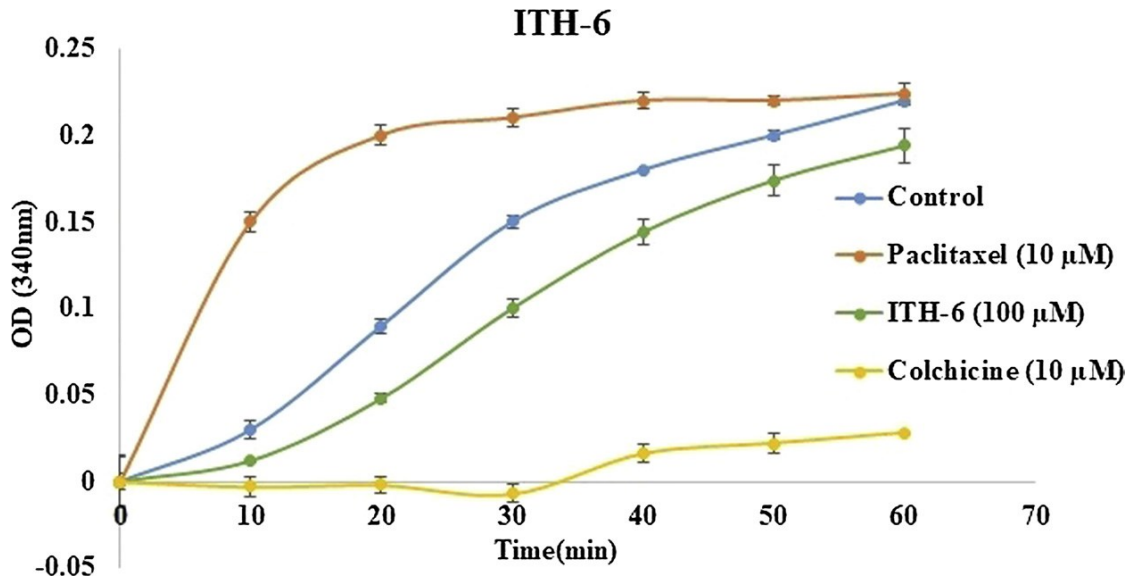
Figure 5. **Effect of ITH-6 on the tubulin polymerization.** The tubulin polymerization assay was performed as per manufacturer's protocol. The change in optical density (OD) at 340 nm was plotted against time in min for ITH-6 at 100 μM (green) was compared with control (blue), paclitaxel at 10 μM (orange), and colchicine at 10 μM (yellow). Points with error bars represent the mean ± SD for independent determinations in triplicates. The figure is a representative of three independent experiments.
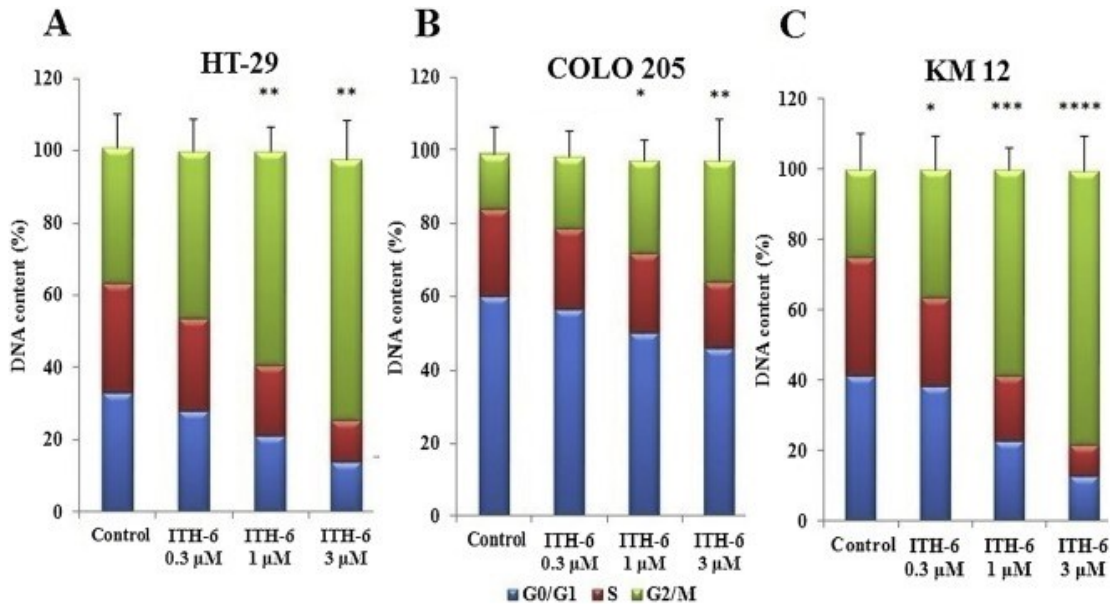
Figure 6

Figure 6. Effect of ITH-6 on the apoptosis of HT-29, COLO 205, and KM 12 cell lines.

(A) HT-29, **(B)** COLO 205, and **(C)** KM 12 cells were treated with ITH-6 (24 h) in a concentration-dependent manner, stained with Annexin-V and PI, and analyzed by flow cytometer. The apoptotic cell population was quantified by flow cytometry. Bar graphs in blue represents live cells, in red represents cells undergoing apoptosis, and in green represents cell undergoing necrosis. Bar graphs represents average cell population of three independent experiments and error bars represents SD for independent determinations in triplicates. ** $p < 0.01$, *** $p < 0.001$, **** $p < 0.0001$ compared to the control group.

Figure 7
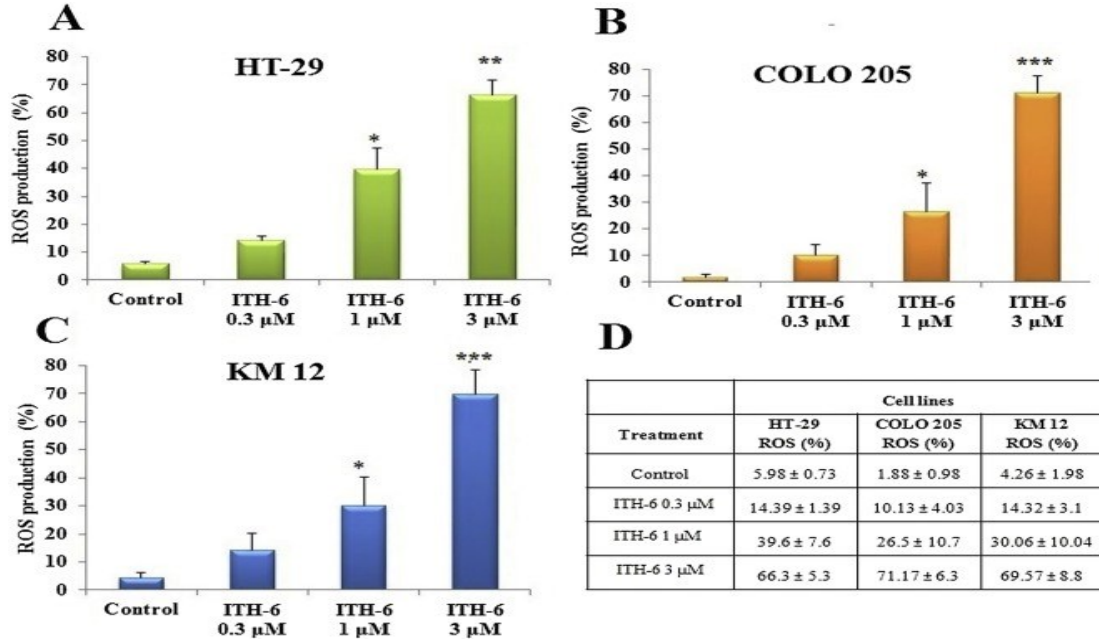
Figure 7. Effect of ITH-6 on the ROS production in HT-29, COLO 205, and KM 12 cell lines. (A) HT-29, **(B)** COLO 205, and **(C)** KM 12 cells were treated with ITH-6 (24 h) in a concentration-dependent manner as mentioned in "Materials and methods". Points with error bars represent the mean $\pm$ SD for independent determinations in triplicates. The figures are representative of three independent experiments.* $p < 0.05$, ** $p < 0.01$ and *** $p < 0.001$ compared to the control group.
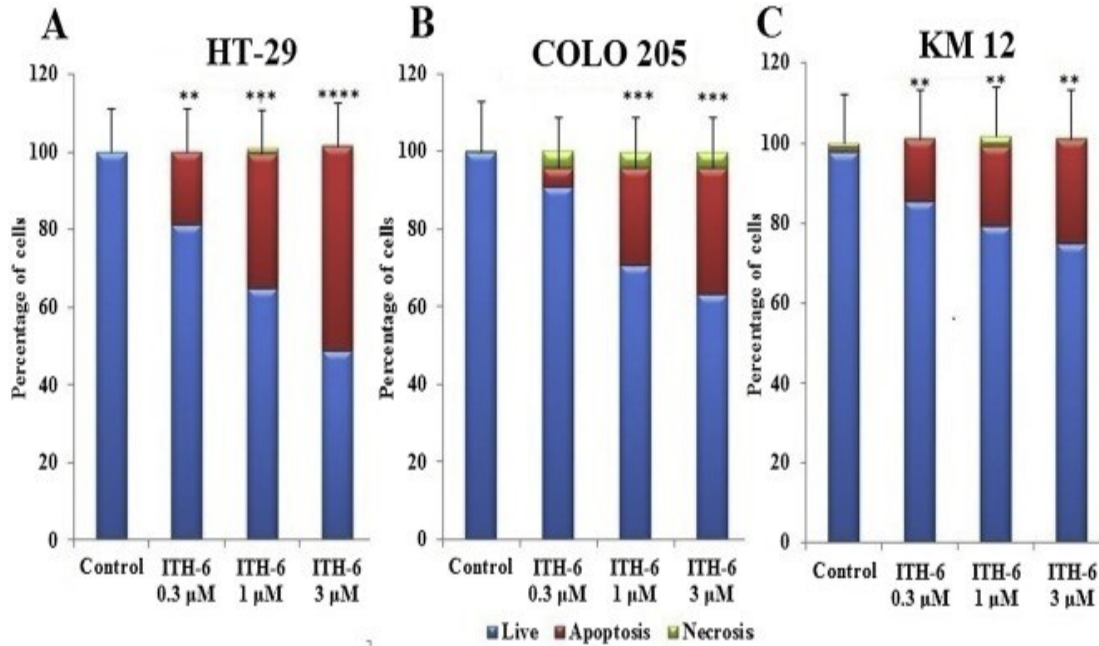
Figure 8
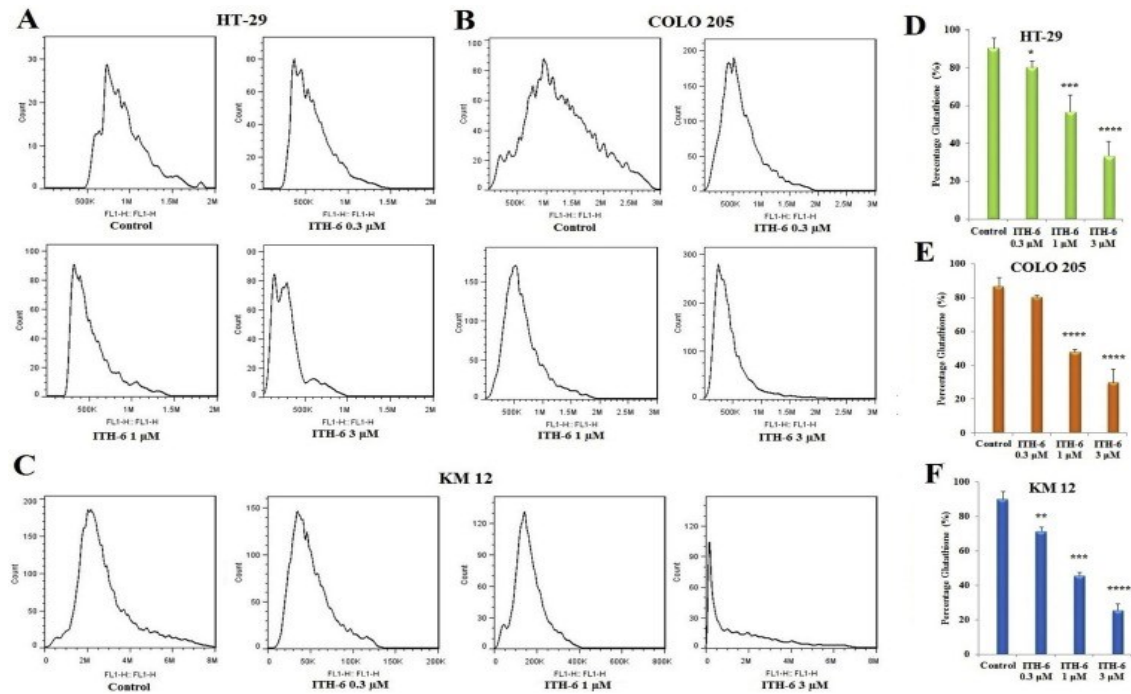
Figure 8. Effect of ITH-6 on the GSH levels of HT-29, COLO 205, and KM 12 cell lines. The GSH assay was performed as per manufacturer's protocol. **(A)** HT-29, **(B)** COLO 205, and **(C)** KM 12 cells were treated with ITH-6 (24 h) in a concentration-dependent manner as mentioned in "Materials and methods". Points with error bars represent the mean ± SD for independent determinations in triplicates. The figures are representative of three independent experiments. * $p < 0.05$, ** $p < 0.01$, *** $p < 0.001$ and **** $p < 0.0001$ compared to the control group.

Figure 9
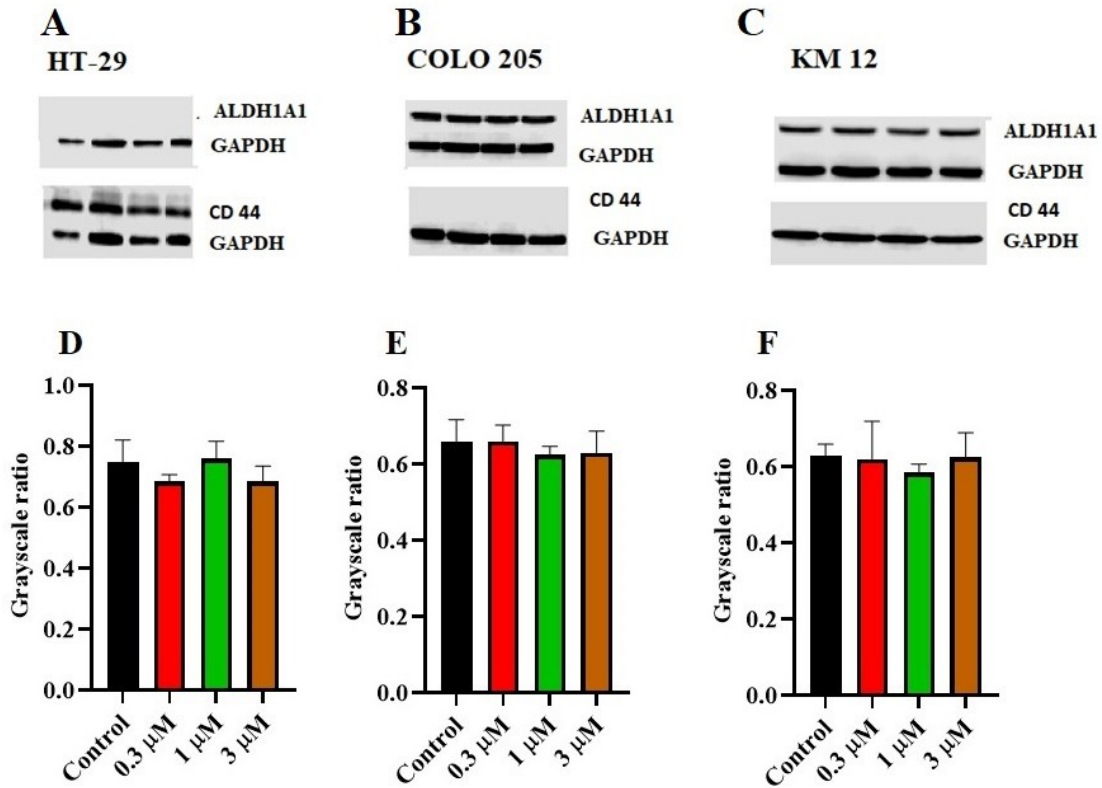
Figure 9. Effect of ITH-6 on the expression of ALD1HA1 and CD44: The effect of ITH-6 on the expression of ALDHA1 and CD44 on **(A)** HT-29 **(B)** COLO 205 and **(C)** KM 12 cells were tested after the cells were treated with 0.3, 1 and 3 µM of ITH-6 for 72 h. Relative quantification of the effect of ITH-6 on **(D)** CD44 in HT-29 and ALDH1A1 in **(E)** COLO 205 and **(F)** KM 12 cells. The expression levels of the target proteins were normalized to GAPDH. Equal amounts of total cell lysates were used for each sample and a Western blot analysis was performed. The figures are representative of three independent experiments.

Figure 10

Figure 10. Effect of ITH-6 on the expression of (A)nuclear and (B) cytoplasmic fraction of NF-kB p65 protein on HT-29 cells. The effect of ITH-6 on the expression of nuclear and cytoplasmic fraction of NF-kB p65 protein was tested after the cells were treated with 0.3, 1 and 3 μM of ITH-6 for 72 h. Relative quantification of the effect of ITH-6 on **(C)** nuclear and **(D)** cytoplasmic fraction of NF-kB p65 in HT-29 cells. The expression level of NF-kB p65 protein was normalized to TBP (nucleus) and GAPDH (cytoplasm). Equal amounts of total cell lysates were used for each sample and a Western blot analysis was performed. The figures are representative of three independent experiments. $* p < 0.05$ compared to the control group

Figure 11

Figure 11. Effect of ITH-6 on the expression of (A) nuclear and (B) cytoplasmic fraction of NF-kB p65 protein on COLO 205 cells. The effect of ITH-6 on the expression of nuclear and cytoplasmic fraction of NF-kB p65 protein was tested after the cells were treated with 0.3, 1 and 3 μM of ITH-6 for 72 h. Relative quantification of the effect of ITH-6 on **(C)** nuclear and **(D)** cytoplasmic fraction of NF-kB p65 in COLO 205 cells. The expression level of NF-kB p65 protein was normalized to TBP (nucleus) and GAPDH (cytoplasm). Equal amounts of total cell lysates were used for each sample and a Western blot analysis was performed. The figures are representative of three independent experiments. * $p < 0.05$ compared to the control group.
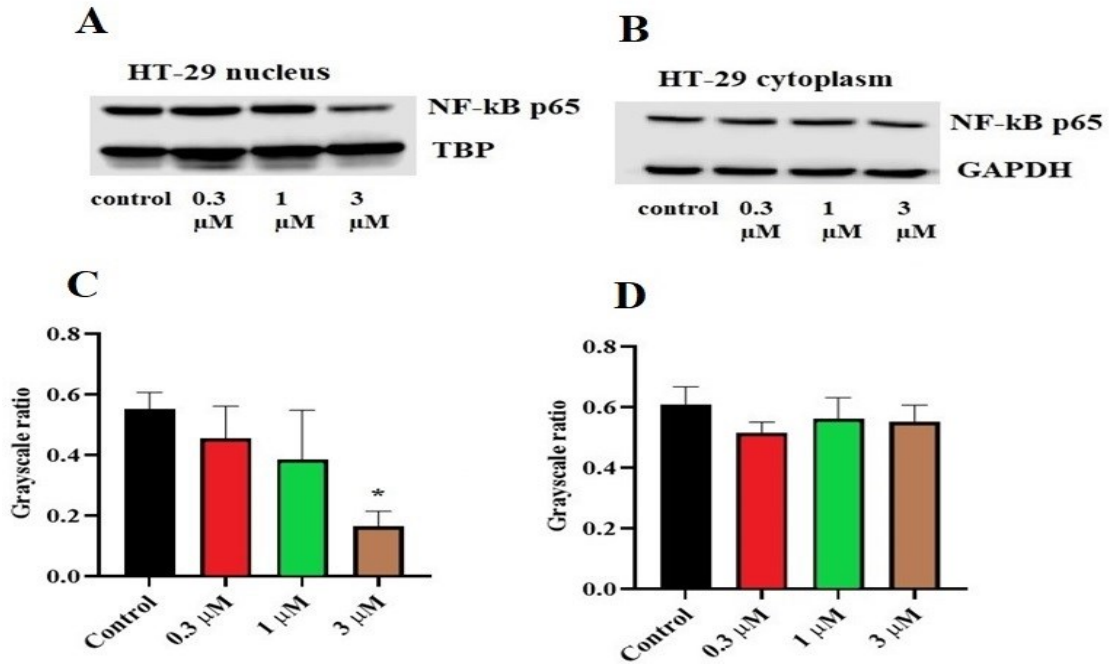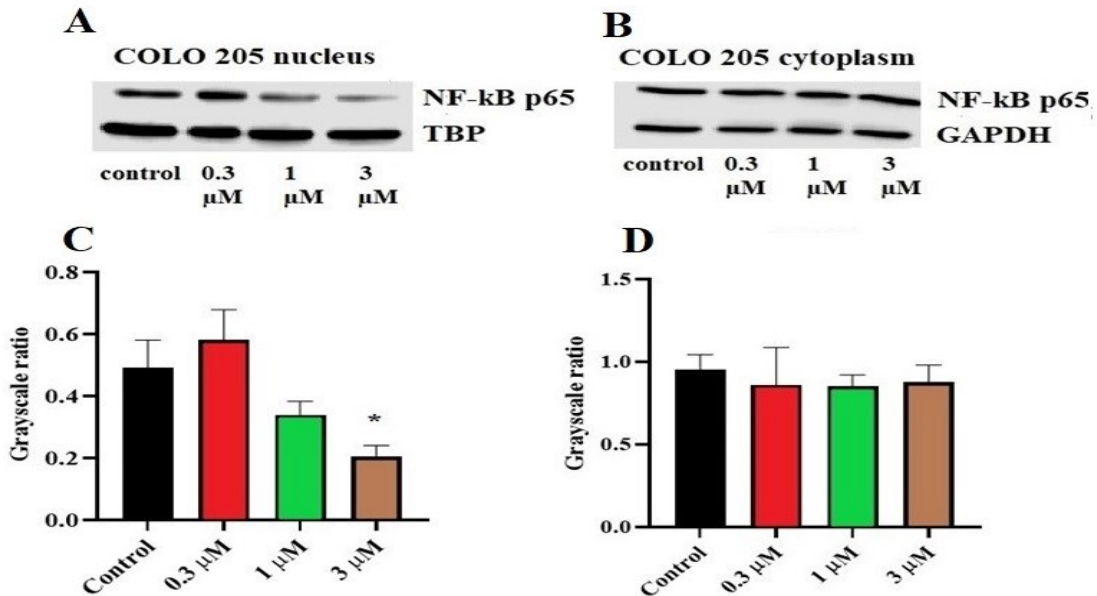
Figure 12
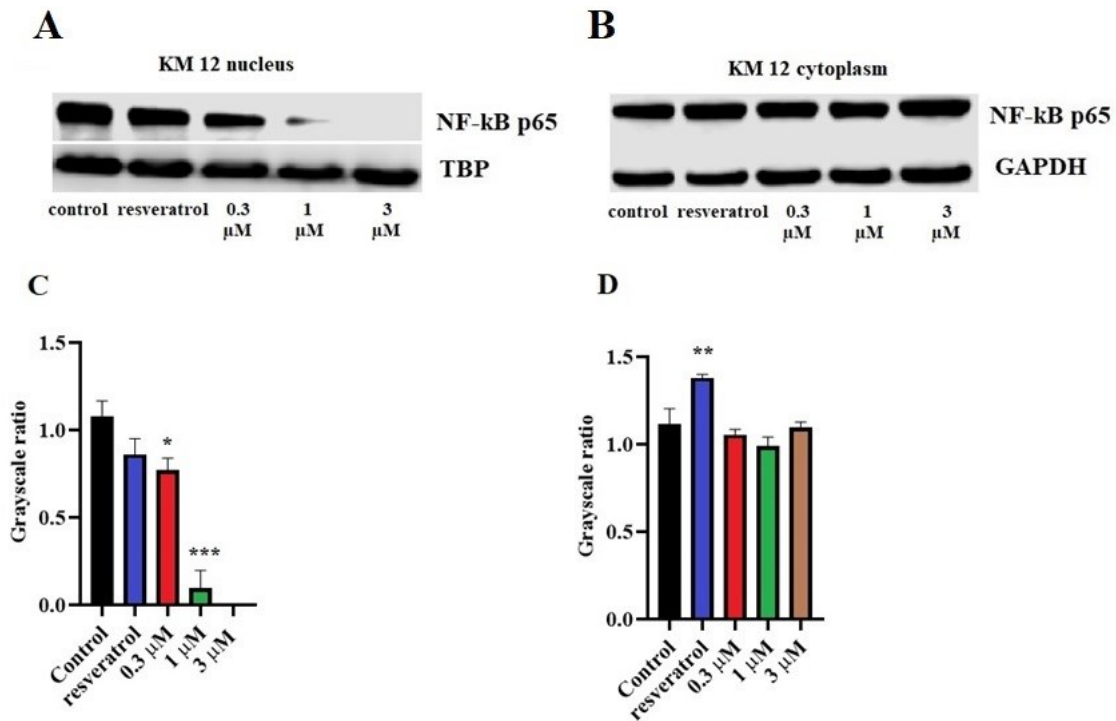
Figure 12. Effect of ITH-6 on the expression of (A) nuclear and (B) cytoplasmic fraction of NF-kB p65 protein on KM 12 cells. The effect of ITH-6 on the expression of nuclear and cytoplasmic fraction of NF-kB p65 protein was tested after the cells were treated with 0.3, 1 and 3 µM of ITH-6 for 72 h. Relative quantification of the effect of ITH-6 on **(C)** nuclear and **(D)** cytoplasmic fraction of NF-kB p65 in KM 12 cells. The expression level of NF-kB p65 protein was normalized to TBP (nucleus) and GAPDH (cytoplasm). Equal amounts of total cell lysates were used for each sample and a Western blot analysis was performed. The figures are representative of three independent experiments. $* p < 0.05$, $** p < 0.01$ and $*** p < 0.001$ compared to the control group.

Figure 13

Figure 13. Effect of ITH-6 on the expression of (C) Topoisomerase I and Procaspase-3 and (A) nuclear and (B) cytoplasmic expression of IkBα on HT-29 cells. The effect of ITH-6 on the expression of Topoisomerase I, Procaspase-3 and IkBα (nuclear and cytoplasmic) was tested after the cells were treated with 0.3, 1 and 3 μM of ITH-6 for 72 h. Relative quantification of the effect of ITH-6 on **(D)** cytoplasmic IkBα, **(E)** Topoisomerase I and **(F)** Procaspase-3 in HT-29 cells. The expression levels of the target proteins were normalized to TBP (nucleus) and GAPDH (cytoplasm). Equal amounts of total cell lysates were used for each sample and a Western blot analysis was performed. The figures are representative of three independent experiments.

Figure 14

Figure 14. Effect of ITH-6 on the expression of (C) Topoisomerase I and Procaspase-3 and (A) nuclear and (B) cytoplasmic expression of IkBα on COLO 205 cells. The effect of ITH-6 on the expression of Topoisomerase I, Procaspase-3 and IkBα (nuclear and cytoplasmic) was tested after the cells were treated with 0.3, 1 and 3 µM of ITH-6 for 72 h. Relative quantification of the effect of ITH-6 on **(D)** cytoplasmic IkBα, **(E)** Topoisomerase I and **(F)** Procaspase-3 in COLO 205 cells. The expression levels of the target proteins were normalized to TBP (nucleus) and GAPDH (cytoplasm). Equal amounts of total cell lysates were used for each sample and a Western blot analysis was performed. The figures are representative of three independent experiments.
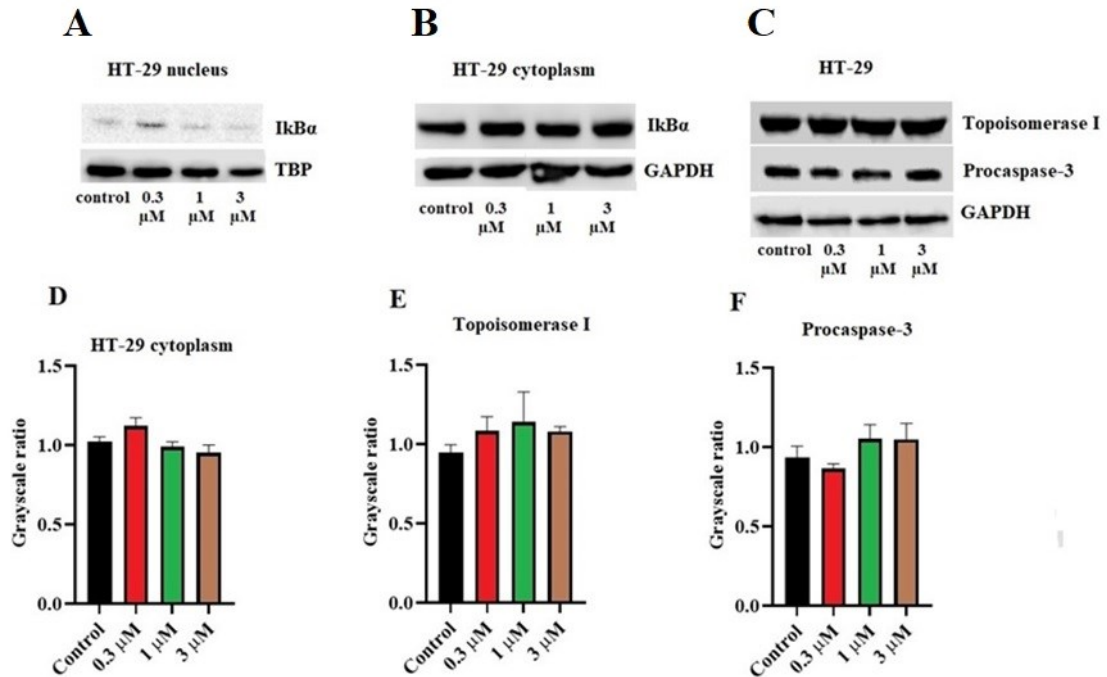
Figure 15
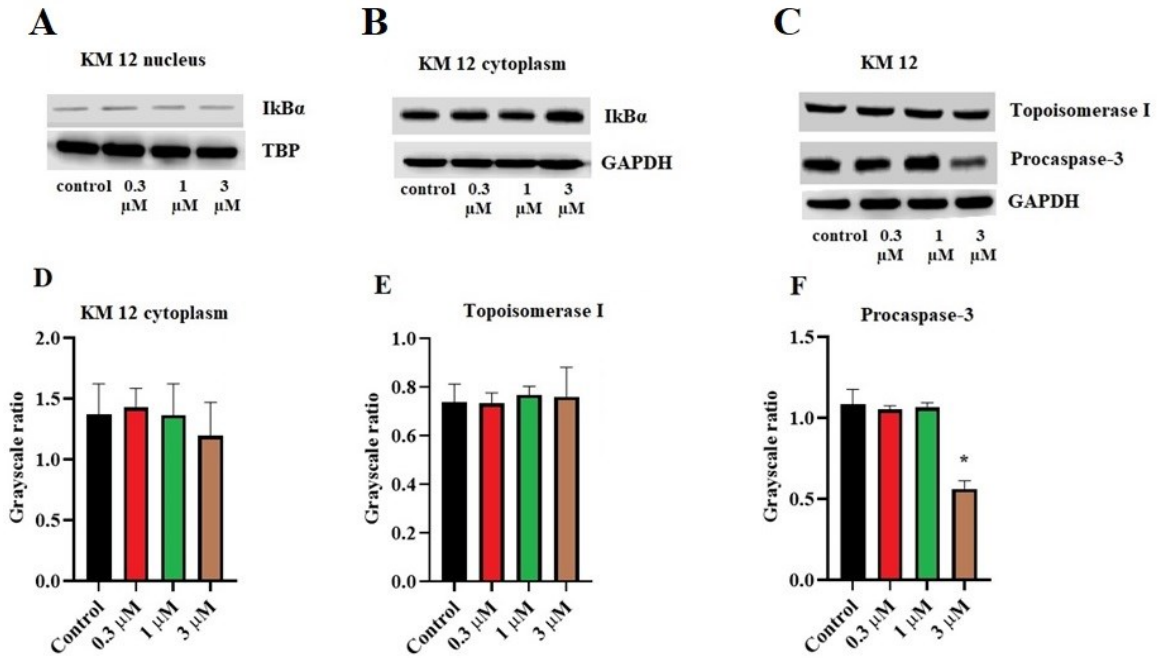
Figure 15. Effect of ITH-6 on the expression of (C) Topoisomerase I and Procaspase-3 and (A) nuclear and (B) cytoplasmic expression of IkBα on KM 12 cells. The effect of ITH-6 on the expression of Topoisomerase I, Procaspase-3 and IkBα (nuclear and cytoplasmic) was tested after the cells were treated with 0.3, 1 and 3 µM of ITH-6 for 72 h. Relative quantification of the effect of ITH-6 on **(D)** cytoplasmic IkBα, **(E)** Topoisomerase I and **(F)** Procaspase-3 in KM 12 cells. The expression levels of the target proteins were normalized to TBP (nucleus) and GAPDH (cytoplasm). Equal amounts of total cell lysates were used for each sample and a Western blot analysis was performed. The figures are representative of three independent experiments. $* p < 0.05$ compared to the control group.
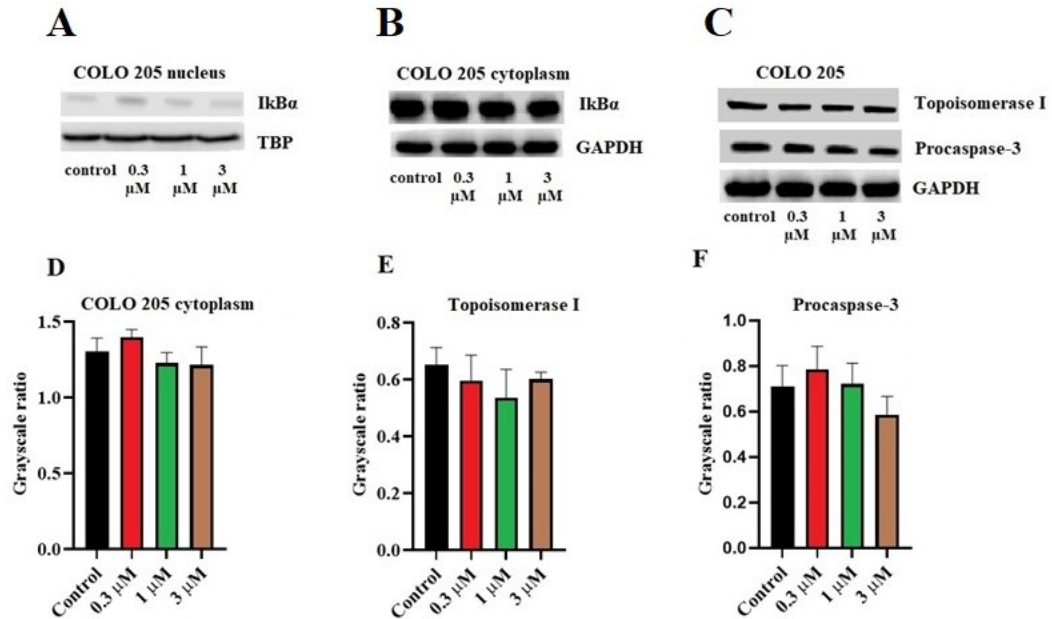
Figure 16
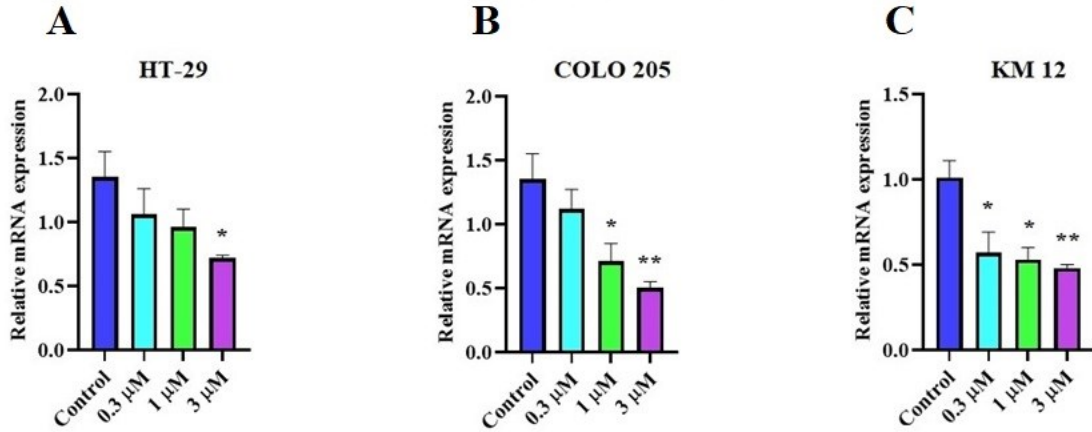
Figure 16. Effect of ITH-6 on NF-kB p65 expression at mRNA level on (A) HT-29, (B) COLO 205, and (C) KM 12 cells. The effect of ITH-6 on NF-kB p65 mRNA expression was tested after the cells were treated with 0.3, 1 and 3 µM of ITH-6 different concentrations for 72 h. Points with error bars represent the mean ± SD for independent determinations in triplicates. The figures are representative of three independent experiments. $*\ p < 0.05$ and $**\ p < 0.01$ compared to the control group.

Figure 17

IL-6 mRNA expression
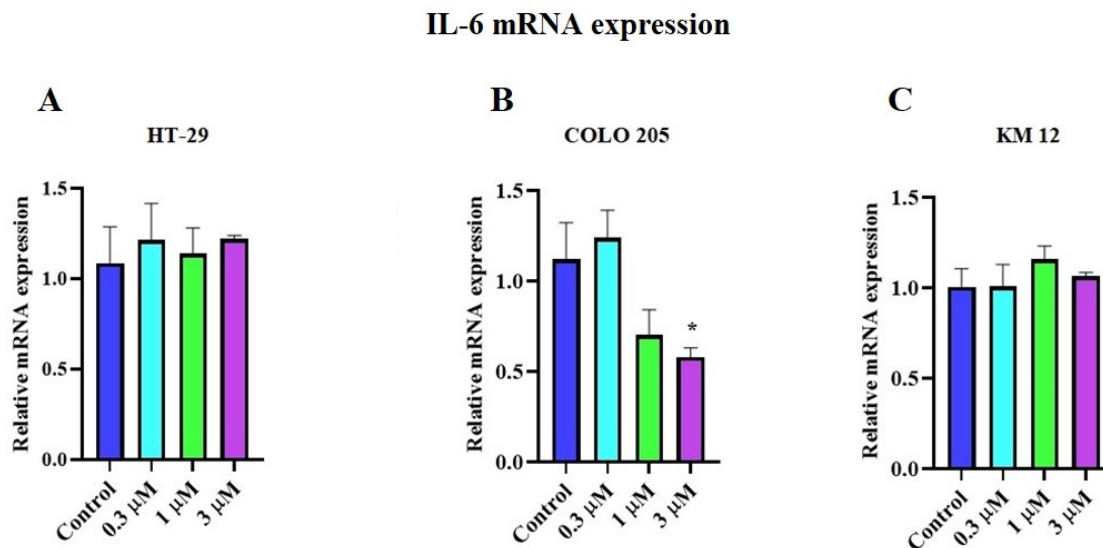
Figure 17. Effect of ITH-6 on IL-6 expression at mRNA level on (A) HT-29, (B) COLO 205, and (C) KM 12 cells. The effect of ITH-6 on IL-6 mRNA expression was tested after the cells were treated with 0.3, 1 and 3 μM of ITH-6 different concentrations, for 72 h. Points with error bars represent the mean ± SD for independent determinations in triplicates. The figures are representative of three independent experiments. * $p < 0.05$ compared to the control group.

Figure 18
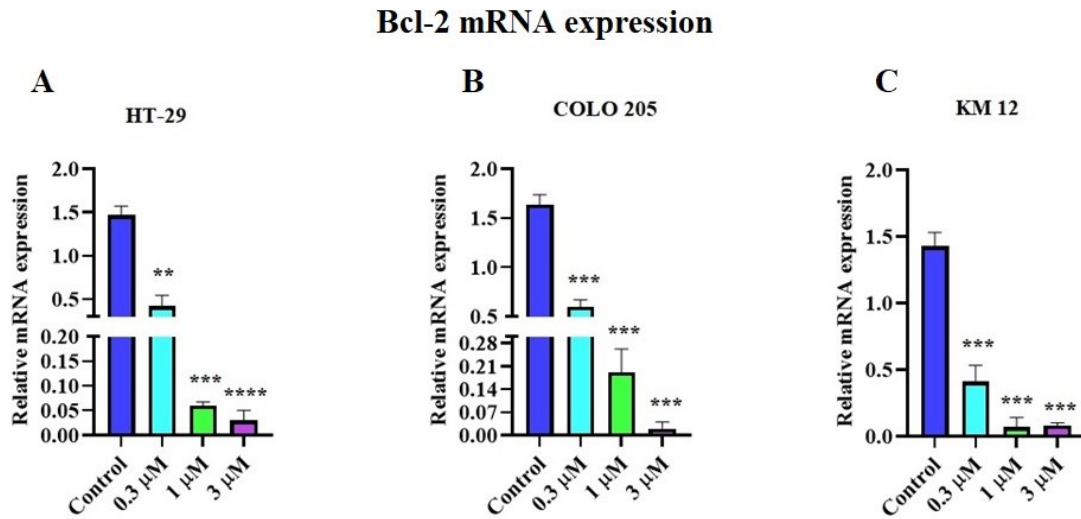
Figure 18. Effect of ITH-6 on Bcl-2 expression at mRNA level on (A) HT-29, (B) COLO 205, and (C) KM 12 cells. The effect of ITH-6 on Bcl-2 mRNA expression was tested after the cells were treated with 0.3, 1 and 3 μM of ITH-6 different concentrations, for 72 h. Points with error bars represent the mean ± SD for independent determinations in triplicates. The figures are representative of three independent experiments. ** $p < 0.01$, *** $p < 0.001$ and **** $p < 0.0001$ compared to the control group.

Figure 19
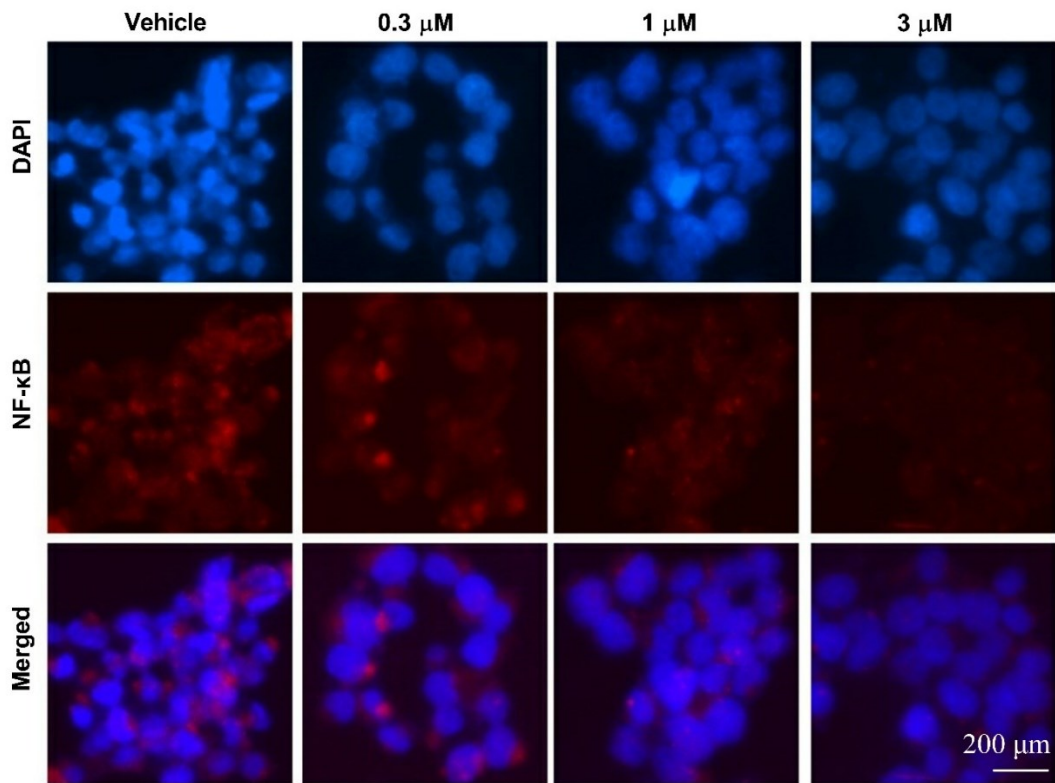
Figure 19. Immunofluorescence experiment on NF-kB p65 expression on HT-29 cells followed by treatment with ITH-6. HT-29 cells were incubated for 72 h with 0.3, 1 and 3 μM of ITH-6. The red color represents the presents of NF-kB p65 and the blue color represents the nucleus.

Figure 20
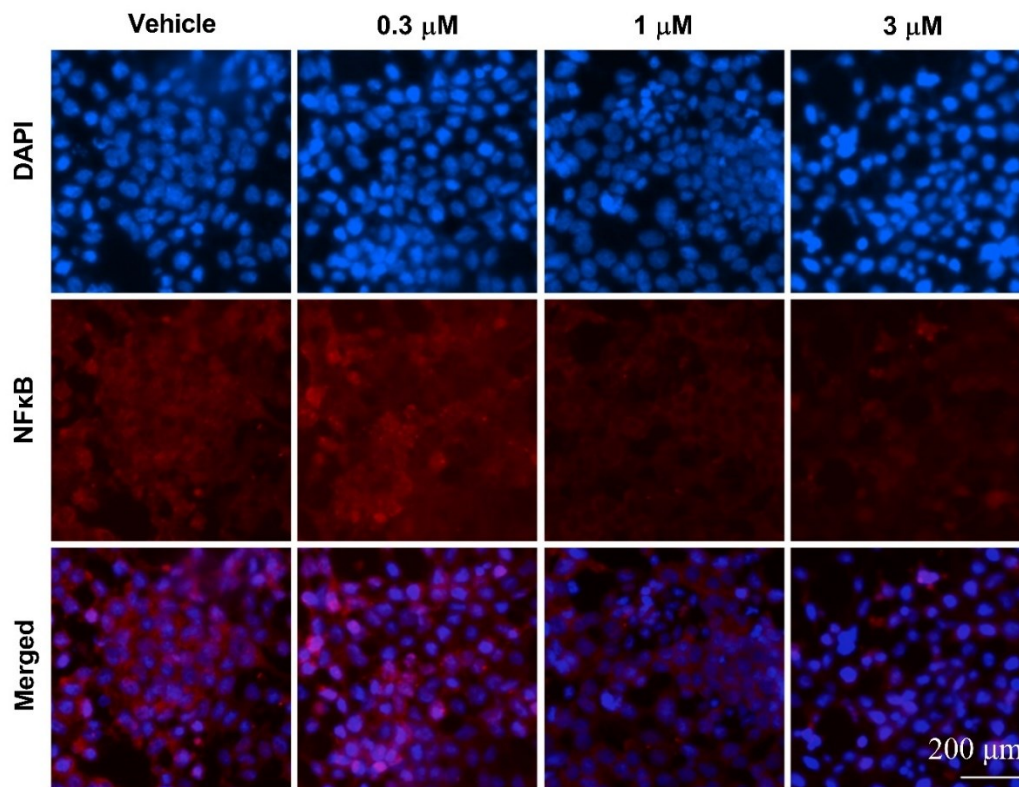
Figure 20. Immunofluorescence experiment on NF-kB p65 expression on COLO 205 cells followed by treatment with ITH-6. COLO 205 cells were incubated for 72 h with 0.3, 1 and 3 µM of ITH-6. The red color represents the presents of NF-kB p65 and the blue color represents the nucleus.

Figure 21
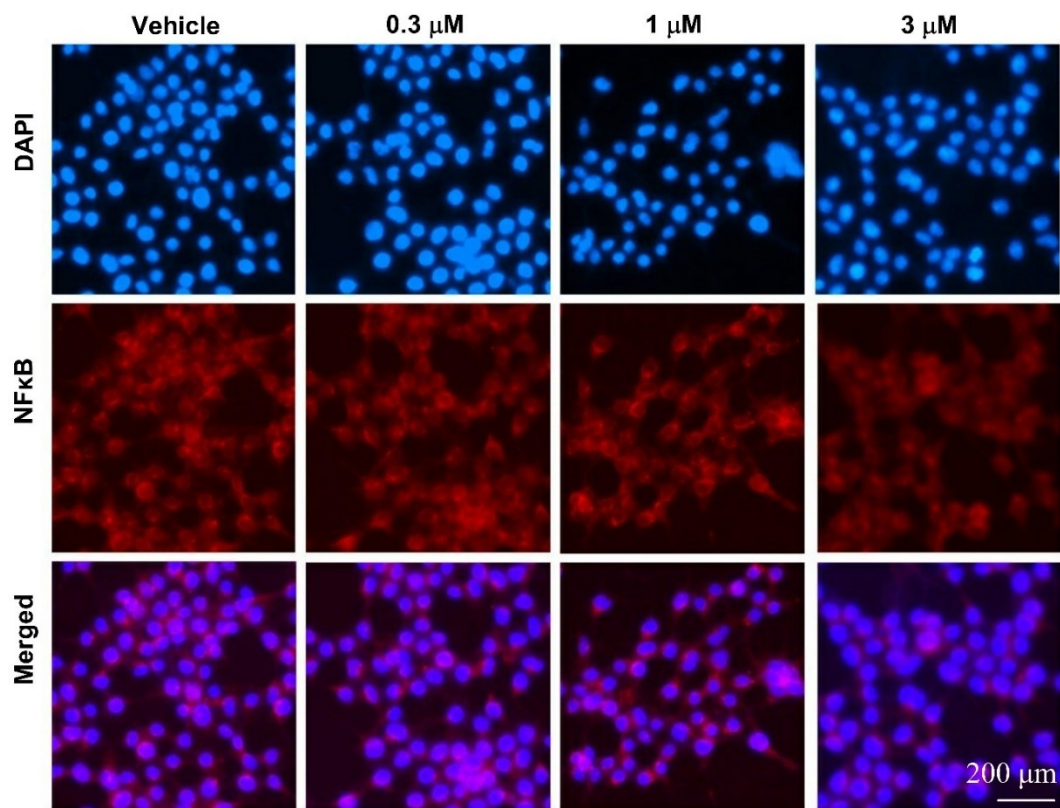
Figure 21. Immunofluorescence experiment on NF-kB p65 expression on KM 12 cells followed by treatment with ITH-6. KM 12 cells were incubated for 72 h with 0.3, 1 and 3 μM of ITH-6. The red color represents the presents of NF-kB p65 and the blue color represents the nucleus.

Figure 22.

Docking study for ITH-6 on NF-kB p65 model

A

B
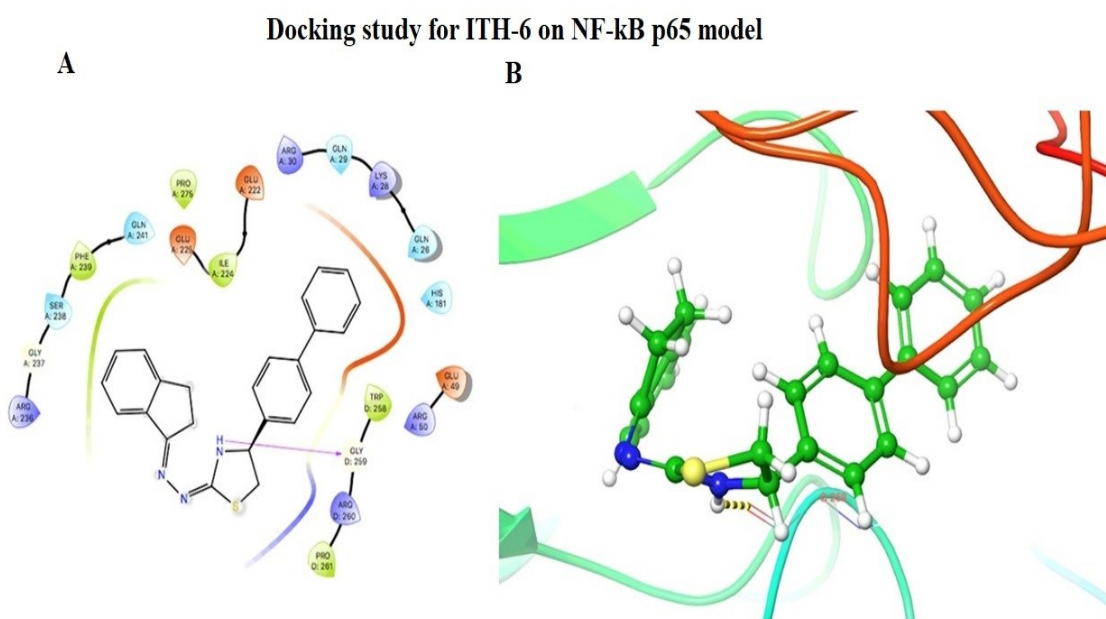
Figure 22. Molecular interaction of ITH-6 with the human NF-kB model. (A)
Docking pose of ITH-6 within the binding pocket of IkBα/NF-kB heterodimer. The
protein is represented as multicolored ribbons. Amino acid residues are shown as follows:
nitrogen in blue, hydrogen in white, carbon in gray, and oxygen in red. The ligand is
represented by the ball and stick model with carbon atoms are represented in carbon in
green, nitrogen in blue, hydrogen in white and sulfur in yellow. the yellow dashes
represent the hydrogen bonding. **(B)** 2-D ligand interaction between ITH-6 and IkBα/NF-

kB heterodimer. Magenta arrow represents hydrogen bonding with amino acid residues within 5 Å of the ligand.

Figure 23
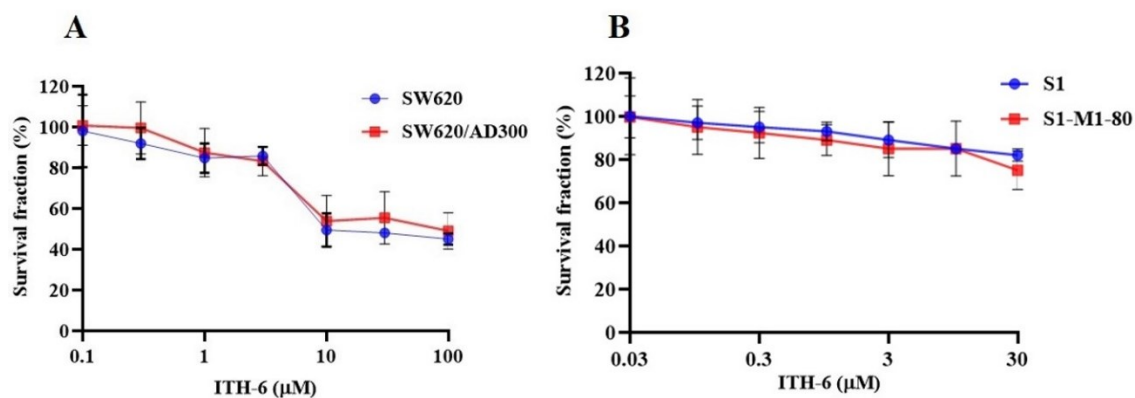
Figure 23. Cytotoxicity of ITH-6 on ABCB1- and ABCG2-overexpressing cell lines. Survival fraction (%) was measured after treatment with ITH-6 (µM) for 72 h on **(A)** SW620, SW620/AD300 and **(B)** S1, S1-M1-80 cell lines. Points with error bars represent the mean ± SD for independent determinations in triplicates. The figures are representative of three independent experiments.

Figure 24
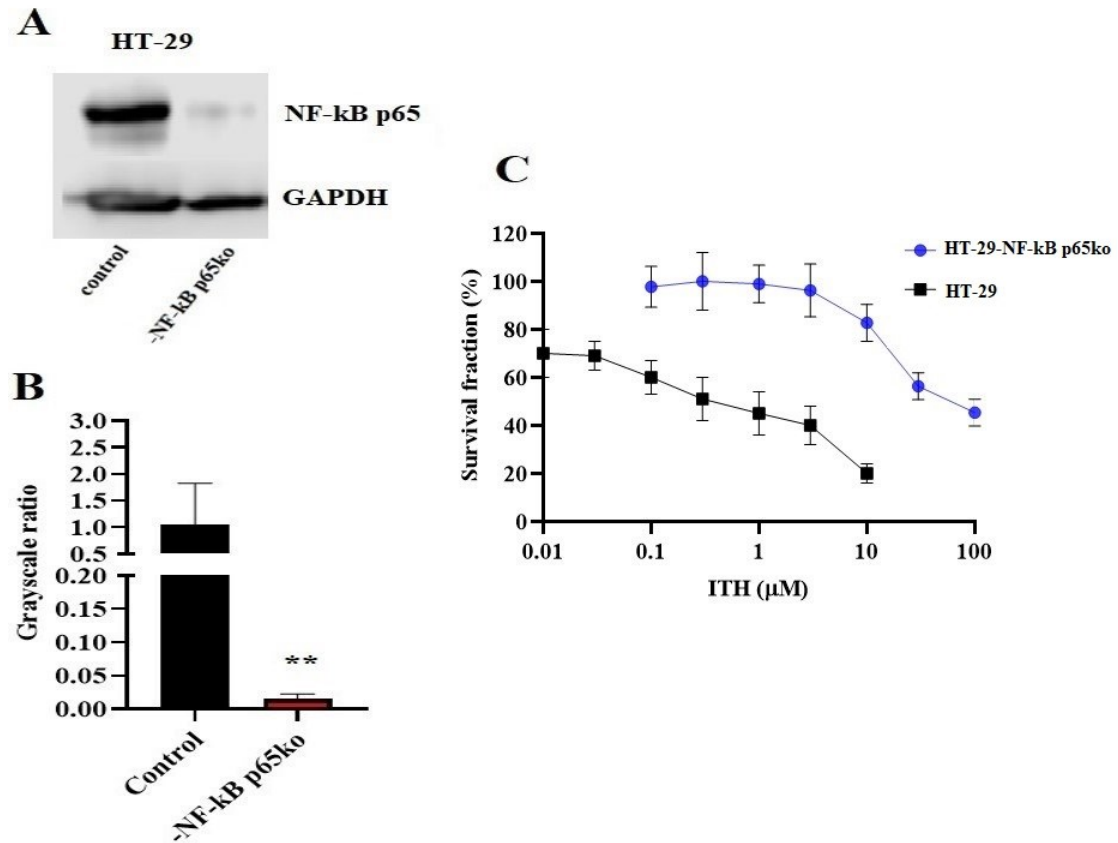
Figure 24. NF-kB p65 gene knockout in HT-29 cells (A) Western blotting result of NF-kB p65 protein expression level and **(B)** relative quantification of NF-kB p65 in HT-29 and HT-29-NF-kB p65ko cells. The expression level of the target protein was normalized to GAPDH. **(C)** Survival fraction (%) was measured after treatment with ITH-6 (μM) for 72 h on HT-29 and HT-29-NF-kB p65ko cells. Points with error bars represent the mean

± SD for independent determinations in triplicates. The figures are representative of three independent experiments. ** $p < 0.01$ compared to the control group.

Figure 25
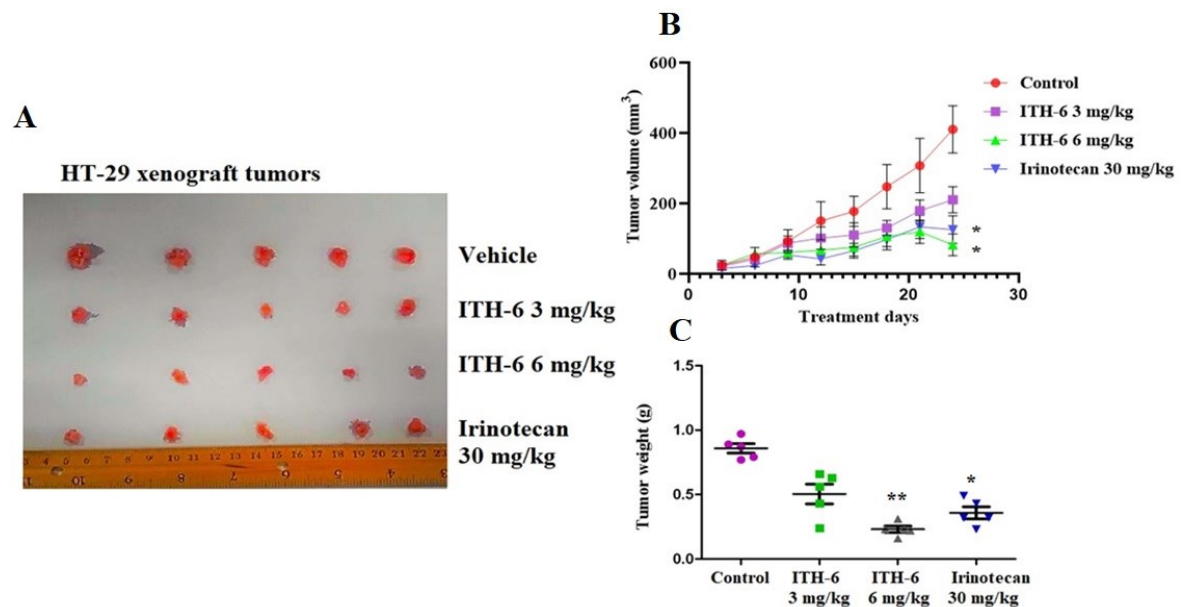
Figure 25. ITH-6 inhibits HT-29 tumor growth, volume, and weight in xenograft mouse model. NCR nude mice were inoculated with subcutaneous implantation of HT-29 cells. During a 21 days treatment period, ITH-6 (6 mg/kg) significantly inhibited the **(A)** growth, **(B)** volume and **(C)** weight of HT-29 tumor xenografts compared to the vehicle control and irinotecan group. Values represent the median ± SD of 6 animals per group. Similar results were obtained in 2 independent experiments. * $p < 0.05$ and ** $p < 0.01$ compared to the control group.

Figure 26
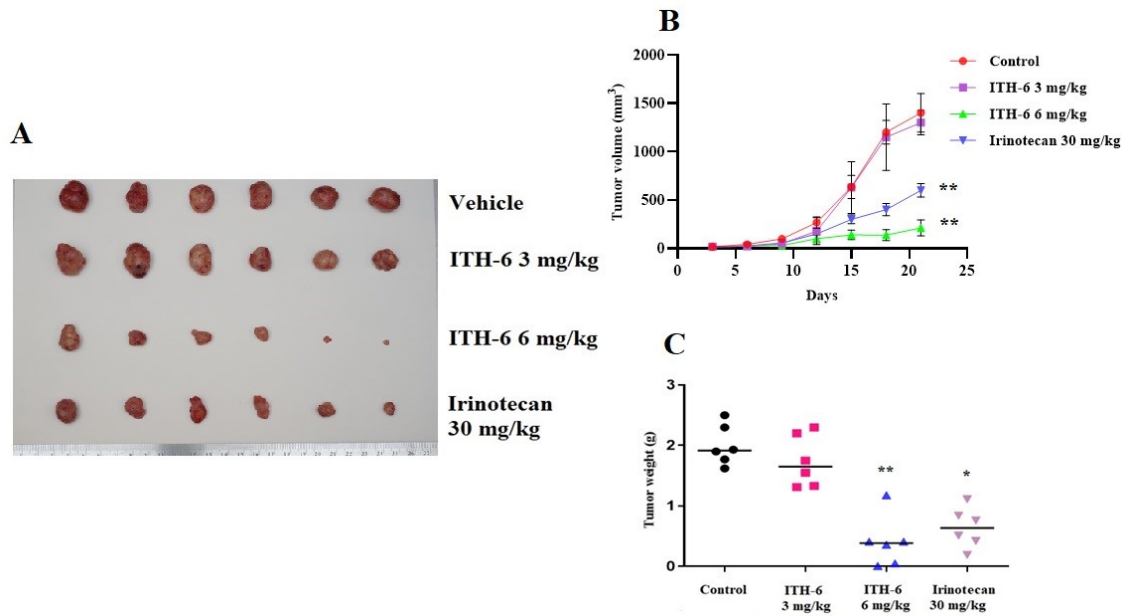
Figure 26. ITH-6 inhibits KM 12 tumor growth, volume, and weight in xenograft mouse model. NCR nude mice were inoculated with subcutaneous implantation of KM 12 cells. During a 21 days treatment period, ITH-6 (6 mg/kg) significantly inhibited the **(A)** growth **(B)** volume and **(C)** weight of KM 12 tumor xenografts compared to the vehicle control and irinotecan group. Values represent the median $\pm$ SD of 6 animals per group. Similar results were obtained in 2 independent experiments. $*$ $p < 0.05$ and $**$ $p < 0.01$ compared to the control group.

Figure 27
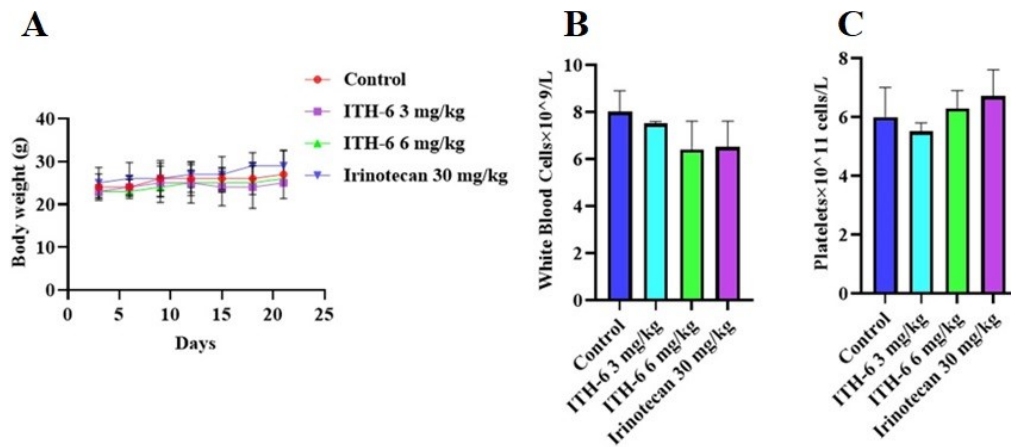
Figure 27. (A) Changes in mean body weight before and after treatment for xenograft model are shown. **(B)** The changes in mean white blood cells in nude mice (n = 6) at the end of the 21-day treatment period and **(C)** the changes in mean platelets in nude mice (n = 6) at the end of the 21-day treatment period.

Figure 28
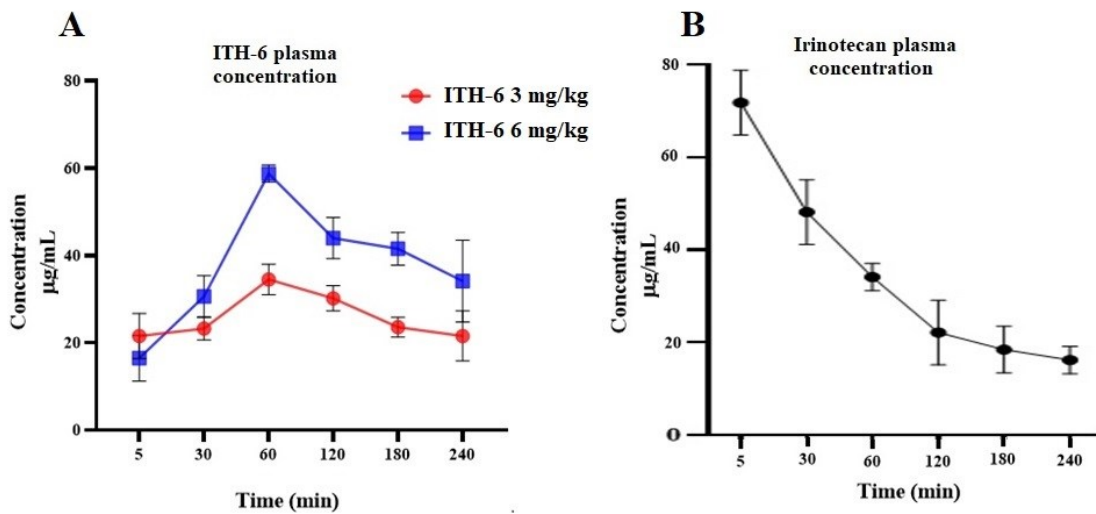
Figure 28. Plasma irinotecan and ITH-6 concentrations in xenograft mouse model

The plasma concentrations at different time points, 5, 30, 60-, 120-, 180- and 240-min following administration of **(A)** ITH-6 (3 and 6 mg/kg) given orally and **(B)** irinotecan (30 mg/kg) given intraperitoneally.

Figure 29
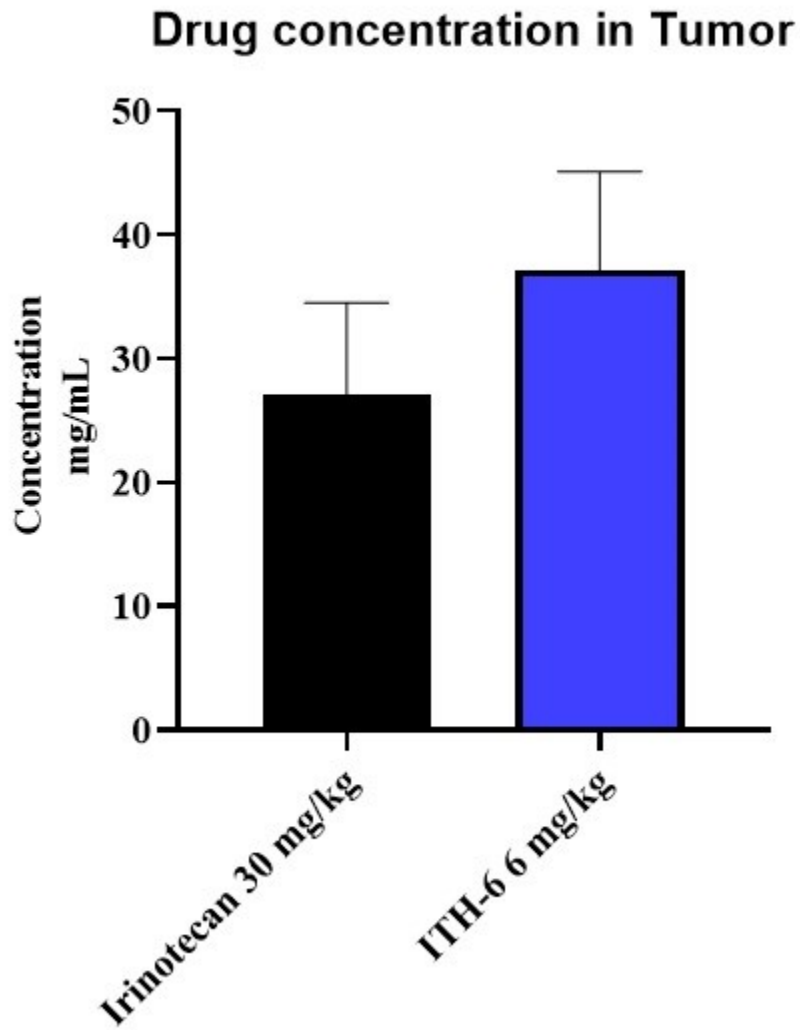
Figure 29. Intratumoral concentrations of irinotecan and ITH-6 in KM 12 (n=6) and

HT-29 tumors (n=6). Points with error bars represent the mean ± SD.

CHAPTER 4. Discussion

Despite of the advances in chemotherapy, the mortality rate of CRC is quite alarming. Patients with CRC fall into two categories; ones in which the disease is confined to the primary site of origin (Dukes' A and B) and the other where it spreads to the regional lymph nodes (Dukes' C and D). The first category of patients can be surgically cured while for the later ones, surgery has is only palliative role and survival rate is less than 30%(81). The drugs already approved and being used for the treatment of colon cancer include irinotecan, oxaliplatin, capecitabine and the targeted drugs include bevacizumab, ramucirumab etc. Irinotecan, approved by the USFDA in 1996, is a prodrug which is converted into its active metabolite, SN-38 inside the body. It has long been used as the first line therapy for patients with recurrent and metastatic CRC however, the dose related toxicities such as vomiting, dehydration, myelosuppression, alopecia, and diarrhea are a serious concern(82). Bevacizumab, a humanized monoclinal antibody was approved by the USFDA in 2004 for the treatment of patients with advanced CRC. Bevacizumab exhibits some rare serious adverse effects such as bowel perforation, arterial embolic events, and leukoencephalopathy (83–85).

In the present study, we find that the compound ITH-**6** has lower IC_{50} values on the colon cancer cell lines, HT-29, COLO 205, and KM 12 as compared to the conventional anticancer drug, irinotecan. Indanone and its derivatives are well known for their wide range of biological activity(28). Studies done in the past have shown that the indanone derivative are potent anti-inflammatory, analgesic, antimicrobial, anticholinergic, anticancer, and antimalarial agents. 3-aryl substituted indanone analog was found significantly active against the HeLa and K562 cell lines(86). The other derivatives, gallic

acid based indanone analogs are cytotoxic (IC_{50} of 0.01 µM) on breast cancer cell lines MCF-7 and MDA-MB-231(36). In addition, 2-substituted indanone analogs are active against non-small lung cancer cell line(87) and 5,6-dimethoxy-1-indanonederivative is significantly cytotoxic on multidrug resistant cell lines, MCF-7/ADR, MES-SA/DX5 and HL-60/ADR(28). The present indanone derivative, ITH-**6** exhibited IC_{50} values of 0.44 µM, 0.98 µM, and 0.41 µM on HT-29, COLO 205, and KM 12 cell lines respectively. The IC_{50} of regorafenib and irinotecan on HT-29, COLO 205, and KM 12 cell lines (22.7 µM, 9.43 µM and 5.02 µM for regorafenib and 8.49 µM, 22.84 µM and 23.15 µM for irinotecan) has shown that ITH-**6** exhibited lower IC_{50} as compared to the newer drugs, regorafenib and irinotecan. The difference in response to different colon cancer cell lines are due to their establishment from different origin and p53 mutation status. Inhibition of the cell proliferation has long been known to be associated with the changes in the cell cycle(88). The alterations in the cell cycle progression cause tumor growth and proliferation. It has been stated that anticancer drugs can arrest the cells in various phases of cell cycle and inhibit the tumor growth(89). Our cell cycle results indicate that ITH-**6** arrest the cells in G2/M phase and the maximum effect is at high concentration (3 µM) and there is no significant effect on other phases of cell cycle. These cell cycle results show that the test compound is G2/M phase specific. This instigated the idea to investigate the effects of ITH-**6** on tubulin polymerization and mitotic spindle formation, two processes that take place in G2/M phases of cell cycle. The tubulin polymerization assay results show that ITH-**6** at 100 µM inhibits tubulin polymerization for 1 h. Paclitaxel (Taxol), a well-known anticancer drug, stabilizes the microtubule against depolymerization, and is hence known as polymerization enhancer(90). Colchicine on the other hand, inhibits the microtubule

polymerization and is thus known as a polymerization inhibitor(91). We compared the tubulin polymerization effects of ITH-**6** to that of paclitaxel and colchicine and found that, like colchicine, ITH-**6** inhibited the tubulin polymerization. However, the extent of inhibition was not significantly comparable.

Since the cell cycle arrest is related to apoptosis, an apoptotic analysis was carried out using HT-29, COLO 205, and KM 12 cell lines. In all the three cell lines, a substantial number of apoptotic cells were observed in the lower and upper right quadrants, which are the representatives of early and late apoptosis. The results showed an increase in early and late apoptosis in these cell lines with maximum apoptosis seen at the highest concentration of 3 μM. Cellular studies have shown that an increase in the level of ROS causes an oxidative stress which results in oxidative damage to the cellular components(92). It enters into the cells, gets converted into the fluorescent (5-chloromethyl-20-7'-dichlorofluorescein (DCF)) product by the action of intracellular peroxides, hence, the ROS analysis is conducted in all the cell lines(93,94). We found that ITH-**6** at the highest concentration (3 μM) induced intracellular ROS production in HT-29, COLO 205, and KM 12 cell lines. The mitochondrial GSH maintains the integrity of mitochondrial proteins and lipids and modulates ROS production. Oxidative damage is associated with an increase in mitochondrial ROS production and a decrease in GSH which in turn triggers apoptosis(95). Therefore, intracellular GSH assay was performed in all the three colon cancer cell lines. A significant decrease in GSH levels was also observed with compound ITH-**6** in all the three cell lines with the maximum decrease at the highest concentration of 3 μM. Given that the cytotoxicity on colon cancer cells could have resulted from an inhibition of some specific proteins related to the apoptotic pathway, we conducted Western blotting and RT-

PCR experiments to determine the mechanism of ITH-6. One of the targeted proteins, NF-kB p65 is a key mediator in inflammation and cancer. Many indanone derivatives which are anticancer agents are proven to downregulate the expression of NF-kB p65 protein. Our results indicated that the incubation of the HT-29, COLO 205, and KM 12 cancer cells with 3 µM of ITH-6 for 72 h significantly decreased the expression of the nuclear fraction of NF-kB p65 protein compared to cells incubated with vehicle and the downregulation is more predominant compared to 20 µM of the positive control, resveratrol. There was no significant change in the cytoplasmic level of NF-kB p65 protein (inactive form which is bound to IkBα). The NF-kB p65 subunit exists in an inactive state in the cytoplasm (96–98) and when stimulated by molecules such as TNFα, or other cell stressors, leads phosphorylation of IkBα, and subsequently results in IkB ubiquitination and degradation. Once degraded, the remaining NF-kB p65 translocates to the nucleus, where it binds to the DNA sequence of various target genes which regulate cell proliferation (99). ITH-6 acts only on the nuclear fraction of NF-kB p65 thus proving it is downregulating the active form of NF-kB p65 protein which plays a role in the cytotoxicity of ITH-6 on these cell lines. Moreover, there was no significant change in the levels of ALDH1A1, CD44, IkBα (nuclear and cytoplasmic), TOP I protein upon treatment with ITH-6.

The effect of ITH-6 may be either on transcriptional or translational level. The incubation of HT-29, COLO 205, and KM 12 cancer cells at various concentrations of ITH-6 for 72 h remarkably decreased the mRNA level of NF-kB p65 compared to cells incubated with vehicle. There was a significant reduction in the mRNA expression of Bcl-2, which is an anti-apoptotic protein and a downstream molecule of NF-kB pathway and overexpression of Bcl-2 is common in a variety of cancers and has been shown to confer resistance to the

apoptotic effect of chemo- and radiotherapy(100). Consequently, we performed *in vitro* immunofluorescent experiments after treating the cells with the test compound, ITH-6 for a period of 72 h. Our results showed that incubation with ITH-6 for a time point of 72 h decreased NF-kB p65 expression which is consistent with the Western blot and mRNA expression results. Furthermore, cytotoxicity assays on ABCB1- and ABCG2-overexpressing cell lines showed that there was no significant difference in the IC_{50} values of ITH-6 and it proved that it is not a substrate of ABCB1 or ABCG2 transporter. The results from the gene knockout studies suggested that the NF-kB p65 gene knockout in HT-29-NF-kB p65ko cell line can be useful in investigating whether ITH-6 induced cytotoxicity is related to the downregulation of the target, NF-KB p65 which is highly expressed in p53 mutant colon cancers.

Finally, based on our in vitro results, we conducted preclinical studies to determine the effect of the anticancer effect of ITH-6 on tumor growth in athymic nude mice implanted with HT-29 and KM 12 cells. The oral administration of 6 mg/kg of ITH-6 remarkably attenuated the tumor growth in mice compared to mice treated with irinotecan (30 mg/kg i.p.). Meanwhile, there was no notable change in body weight, WBC, and platelets count, suggesting that ITH-6 can be tolerated at this dose and may be a promising candidate for treating p53 mutant colon cancers. Furthermore, the anticancer efficacy of ITH-6 is better than the positive control, irinotecan which can be further proved by its increased tumor concentration compared to irinotecan. Our *in vivo* results suggest that ITH-6 has a significant anticancer activity in mice with HT-29/KM 12 cancer cell xenografts at a dose that does not produce significant toxic effects.

CHAPTER 5. Conclusion

Anticancer drug discovery and development are considered as the grand challenges for the pharmaceutical industry. Extremely dynamic mitotic-spindle microtubules indeed remain the most successful and promising targets for anticancer therapy. Microtubule-stabilizing agents are continually playing an important role in anticancer drug discovery and development. In this study, we have shown that ITH-**6** is an effective cytotoxic agent against p53 mutant colon cancer cells and exhibits a better cytotoxic effect compared to other drugs approved for colon cancer. Mechanistically, ITH-**6** inhibits tubulin polymerization, alters the cell cycle progression, and induces apoptosis by elevating the intra cellular ROS and decreasing the intracellular GSH levels. It also downregulates the expression of the NF-kB p65 and Bcl-2 in these cell lines which further proves its role in the cytotoxicity of colon cancer cell lines. ITH-6 at a dose of 6 mg/kg p.o., did not produce any observable toxic effects in the *in vivo* tumor xenografted mice during the treatment period. It significantly decreased tumor size, growth rate and tumor volume in mice bearing HT-29 and KM 12 tumor xenografts, compared to irinotecan. Together with its mechanism of action, ITH-**6** could be a potential anticancer drug candidate for p53 mutant CRC treatment.

References

1. Anreddy N, Patel A, Zhang Y-K, Wang Y-J, Shukla S, Kathawala RJ, et al. A-803467, a tetrodotoxin-resistant sodium channel blocker, modulates ABCG2-mediated MDR in vitro and in vivo. Oncotarget [Internet]. 2015 Nov 17;6(36):39276–91. Available from: https://pubmed.ncbi.nlm.nih.gov/26515463

2. Kathawala RJ, Chen J-J, Zhang Y-K, Wang Y-J, Patel A, Wang D-S, et al. Masitinib antagonizes ATP-binding cassette subfamily G member 2-mediated multidrug resistance. Int J Oncol [Internet]. 2014/03/13. 2014 May;44(5):1634–42. Available from: https://pubmed.ncbi.nlm.nih.gov/24626598

3. Gupta P, Jani KA, Yang D-H, Sadoqi M, Squillante E, Chen Z-S. Revisiting the role of nanoparticles as modulators of drug resistance and metabolism in cancer. Expert Opin Drug Metab Toxicol [Internet]. 2016 Mar 3;12(3):281–9. Available from: https://doi.org/10.1517/17425255.2016.1145655

4. Gupta P, Xie M, Narayanan S, Wang Y-J, Wang X-Q, Yuan T, et al. GSK1904529A, a Potent IGF-IR Inhibitor, Reverses MRP1-Mediated Multidrug Resistance. J Cell Biochem [Internet]. 2017/05/03. 2017 Oct;118(10):3260–7. Available from: https://www.ncbi.nlm.nih.gov/pubmed/28266043

5. Mokhtari S, Mosaddegh M, Hamzeloo Moghadam M, Soleymani Z, Ghafari S, Kobarfard F. Synthesis and cytotoxic evaluation of novel 3-substituted derivatives of 2-indolinone. Iran J Pharm Res IJPR [Internet]. 2012;11(2):411–21. Available from: http://europepmc.org/abstract/MED/24250465

6. Arnold M, Sierra MS, Laversanne M, Soerjomataram I, Jemal A, Bray F. Global patterns and trends in colorectal cancer incidence and mortality. Gut, gutjnl-.

2016;2:2015–31091.

7.   Cepowicz D, Zaręba K, Pryczynicz A, Dawidziuk T, Żurawska J, Hołody-Zaręba J, et al. Blood serum levels of E-cadherin in patients with colorectal cancer. Prz Gastroenterol. 12(3):186–191.

8.   Albanes D. Energy balance, body size, and cancer. Crit Rev Oncol Hematol. 10(3):283–303.

9.   Kono S, Handa K, Hayabuchi H, Kiyohara C, Inoue H, Marugame T, et al. Obesity, weight gain and risk of colon adenomas in Japanese men. Jpn J Cancer Res. 90(8):805–811.

10. Moore JR, LaMont JT. Colorectal cancer. Risk factors and screening strategies. Arch Intern Med. 144(9):1819–1823.

11. Gryfe R, Kim H, Hsieh ET, Aronson MD, Holowaty EJ, Bull SB, et al. Tumor microsatellite instability and clinical outcome in young patients with colorectal cancer. N Engl J Med. 342(2):69–77.

12. Wynder EL, Shigematsu T. Environmental factors of cancer of the colon and rectum. Cancer. 20(9):1520–1561.

13. Siegel RL, Miller KD, Jemal A. Cancer statistics, 2020. CA Cancer J Clin [Internet]. 2020 Jan 1;70(1):7–30. Available from: https://doi.org/10.3322/caac.21590

14. O'Brien JM, Denmark, Finland by PL, Holm N V, Verkasalo PK, Iliadou A, et al. Environmental and heritable factors in the causation of cancer: analyses of cohorts of twins from Sweden. J Med. 343(78–84):167–168.

15. Hisamuddin IM, Yang VW. Genetics of colorectal cancer. MedGenMed. 6(3):13.

16. Compton CC. Colorectal carcinoma: diagnostic, prognostic, and molecular features. Mod Pathol. 16(4):376–388.

17. Schuell B, Gruenberger T, Kornek G V, Dworan N, Depisch D, Lang F, et al. Side effects during chemotherapy predict tumour response in advanced colorectal cancer. Br J Cancer. 93(7):744–748.

18. Wiela-Hojeńska A, Kowalska T, Filipczyk-Cisarż E, Łapiński Ł, Nartowski K. Evaluation of the toxicity of anticancer chemotherapy in patients with colon cancer. Adv Clin Exp Med. 24(1):103–111.

19. Wang Y-J, Zhang Y-K, Zhang G-N, Al Rihani SB, Wei M-N, Gupta P, et al. Regorafenib overcomes chemotherapeutic multidrug resistance mediated by ABCB1 transporter in colorectal cancer: In vitro and in vivo study. Cancer Lett [Internet]. 2017/03/14. 2017 Jun 28;396:145–54. Available from: https://pubmed.ncbi.nlm.nih.gov/28302530

20. Mirone G, Perna S, Shukla A, Marfe G. Involvement of Notch-1 in Resistance to Regorafenib in Colon Cancer Cells. J Cell Physiol. 231(5):1097–1105.

21. Anreddy N, Gupta P, Kathawala RJ, Patel A, Wurpel JN, Chen ZS. Tyrosine kinase inhibitors as reversal agents for ABC transporter mediated drug resistance. Molecules. 19(9):13848–13877.

22. Kathawala RJ, Gupta P, Ashby CR, Chen ZS. The modulation of ABC transporter-mediated multidrug resistance in cancer: a review of the past decade. Drug Resist Updat. 18:1–17.

23. Ganellin C. Indane and indene derivatives of biological interest. Adv Drug Res. 4:163.

24.   Klaus M. Tetrahydronaphthalene and indane compounds useful as anti-tumor agents. Google Patents;

25.   Vilums M, Heuberger J, Heitman LH, IJzerman AP. Indanes—Properties, Preparation, and Presence in Ligands for G Protein Coupled Receptors. Med Res Rev. 35(6):1097–1126.

26.   Yao S-W, Lopes V, Fernández F, Garcıa-Mera X, Morales M, Rodrıguez-Borges J, et al. Synthesis and QSAR study of the anticancer activity of some novel indane carbocyclic nucleosides. Bioorg Med Chem. 11(23):4999–5006.

27.   Schumann H, Stenzel O, Girgsdies F, Halterman RL. Synthesis and Characterization of (−)-1-Menthyl-4,7-dimethylindene and Its Main Group Metal Compounds with Lithium, Sodium, Potassium, and Tin. Organometallics [Internet]. 2001 Apr 1;20(9):1743–51. Available from: https://doi.org/10.1021/om001074m

28.   Leoni LM, Hamel E, Genini D, Shih H, Carrera CJ, Cottam HB, et al. Indanocine, a microtubule-binding indanone and a selective inducer of apoptosis in multidrug-resistant cancer cells. J Natl Cancer Inst. 92(3):217–224.

29.   Sugimoto H, Ogura H, Arai Y, Limura Y, Yamanishi Y. Research and development of donepezil hydrochloride, a new type of acetylcholinesterase inhibitor. Jpn J Pharmacol. 2002 May;89(1):7–20.

30.   Finkielsztein LM, Castro EF, Fabián LE, Moltrasio GY, Campos RH, Cavallaro L V, et al. New 1-indanone thiosemicarbazone derivatives active against BVDV. Eur J Med Chem. 2008 Aug;43(8):1767–73.

31.   Fillion E, Fishlock D, Wilsily A, Goll JM. Meldrum's acids as acylating agents in

the catalytic intramolecular Friedel-Crafts reaction. J Org Chem. 2005 Feb;70(4):1316–27.

32. Petrignet J, Roisnel T, Grée R. Application of the intramolecular isomerisation-aldolisation from allylic alcohols and allylic silyl ethers to the synthesis of indanones and indenones. Chemistry. 2007;13(26):7374–84.

33. Huang L, Miao H, Sun Y, Meng F, Li X. Discovery of indanone derivatives as multi-target-directed ligands against Alzheimer's disease. Eur J Med Chem. 2014 Nov;87:429–39.

34. Chan L, Pereira O, Reddy TJ, Das SK, Poisson C, Courchesne M, et al. Discovery of thiophene-2-carboxylic acids as potent inhibitors of HCV NS5B polymerase and HCV subgenomic RNA replication. Part 2: tertiary amides. Bioorg Med Chem Lett. 2004 Feb;14(3):797–800.

35. Chan L, Das SK, Reddy TJ, Poisson C, Proulx M, Pereira O, et al. Discovery of thiophene-2-carboxylic acids as potent inhibitors of HCV NS5B polymerase and HCV subgenomic RNA replication. Part 1: Sulfonamides. Bioorg Med Chem Lett. 2004 Feb;14(3):793–6.

36. Saxena HO, Faridi U, Srivastava S, Kumar JK, Darokar MP, Luqman S, et al. Gallic acid-based indanone derivatives as anticancer agents. Bioorg Med Chem Lett. 18(14):3914–3918.

37. Merga YJ, O'Hara A, Burkitt MD, Duckworth CA, Probert CS, Campbell BJ, et al. Importance of the alternative NF-κB activation pathway in inflammation-associated gastrointestinal carcinogenesis. Am J Physiol Liver Physiol [Internet]. 2016 Apr 21;310(11):G1081–90. Available from:

https://doi.org/10.1152/ajpgi.00026.2016

38. Pereira SG, Oakley F. Nuclear factor-kappaB1: regulation and function. Int J Biochem Cell Biol. 2008;40(8):1425–30.

39. Shih VF-S, Tsui R, Caldwell A, Hoffmann A. A single NFκB system for both canonical and non-canonical signaling. Cell Res [Internet]. 2010/11/23. 2011 Jan;21(1):86–102. Available from: https://pubmed.ncbi.nlm.nih.gov/21102550

40. Zhang Q, Lenardo MJ, Baltimore D. 30 Years of NF-κB: A Blossoming of Relevance to Human Pathobiology. Cell [Internet]. 2017 Jan 12;168(1):37–57. Available from: https://doi.org/10.1016/j.cell.2016.12.012

41. Oeckinghaus A, Ghosh S. The NF-kappaB family of transcription factors and its regulation. Cold Spring Harb Perspect Biol. 2009 Oct;1(4):a000034–a000034.

42. Hayden MS, Ghosh S. NF-κB, the first quarter-century: remarkable progress and outstanding questions. Genes Dev. 2012 Feb;26(3):203–34.

43. Hoesel B, Schmid JA. The complexity of NF-κB signaling in inflammation and cancer. Mol Cancer. 2013 Aug;12:86.

44. Song W, Mazzieri R, Yang T, Gobe GC. Translational Significance for Tumor Metastasis of Tumor-Associated Macrophages and Epithelial-Mesenchymal Transition. Front Immunol [Internet]. 2017 Sep 13;8:1106. Available from: https://pubmed.ncbi.nlm.nih.gov/28955335

45. Zhong L, Chen X-F, Wang T, Wang Z, Liao C, Wang Z, et al. Soluble TREM2 induces inflammatory responses and enhances microglial survival. J Exp Med [Internet]. 2017/02/16. 2017 Mar 6;214(3):597–607. Available from: https://pubmed.ncbi.nlm.nih.gov/28209725

46. Vlantis K, Wullaert A, Polykratis A, Kondylis V, Dannappel M, Schwarzer R, et al. NEMO Prevents RIP Kinase 1-Mediated Epithelial Cell Death and Chronic Intestinal Inflammation by NF-κB-Dependent and -Independent Functions. Immunity [Internet]. 2016 Mar 15;44(3):553–67. Available from: https://pubmed.ncbi.nlm.nih.gov/26982364

47. Tosello V, Bordin F, Yu J, Agnusdei V, Indraccolo S, Basso G, et al. Calcineurin and GSK-3 inhibition sensitizes T-cell acute lymphoblastic leukemia cells to apoptosis through X-linked inhibitor of apoptosis protein degradation. Leukemia. 2016 Apr;30(4):812–22.

48. Kwon H-J, Choi G-E, Ryu S, Kwon SJ, Kim SC, Booth C, et al. Stepwise phosphorylation of p65 promotes NF-κB activation and NK cell responses during target cell recognition. Nat Commun [Internet]. 2016 May 25;7:11686. Available from: https://pubmed.ncbi.nlm.nih.gov/27221592

49. Sau A, Lau R, Cabrita MA, Nolan E, Crooks PA, Visvader JE, et al. Persistent Activation of NF-κB in BRCA1-Deficient Mammary Progenitors Drives Aberrant Proliferation and Accumulation of DNA Damage. Cell Stem Cell [Internet]. 2016/06/09. 2016 Jul 7;19(1):52–65. Available from: https://pubmed.ncbi.nlm.nih.gov/27292187

50. Salazar L, Kashiwada T, Krejci P, Meyer AN, Casale M, Hallowell M, et al. Fibroblast growth factor receptor 3 interacts with and activates TGFβ-activated kinase 1 tyrosine phosphorylation and NFκB signaling in multiple myeloma and bladder cancer. PLoS One [Internet]. 2014 Jan 23;9(1):e86470–e86470. Available from: https://pubmed.ncbi.nlm.nih.gov/24466111

51. Hanahan D, Weinberg RA. Hallmarks of Cancer: The Next Generation. Cell [Internet]. 2011 Mar 4;144(5):646–74. Available from: https://doi.org/10.1016/j.cell.2011.02.013

52. Terzić J, Grivennikov S, Karin E, Karin M. Inflammation and colon cancer. Gastroenterology. 2010 Jun;138(6):2101-2114.e5.

53. Colotta F, Allavena P, Sica A, Garlanda C, Mantovani A. Cancer-related inflammation, the seventh hallmark of cancer: links to genetic instability. Carcinogenesis. 2009 Jul;30(7):1073–81.

54. Elinav E, Nowarski R, Thaiss CA, Hu B, Jin C, Flavell RA. Inflammation-induced cancer: crosstalk between tumours, immune cells and microorganisms. Nat Rev Cancer. 2013 Nov;13(11):759–71.

55. Xia Y, Yeddula N, Leblanc M, Ke E, Zhang Y, Oldfield E, et al. Reduced cell proliferation by IKK2 depletion in a mouse lung-cancer model. Nat Cell Biol. 2012 Feb;14(3):257–65.

56. Webster GA, Perkins ND. Transcriptional cross talk between NF-kappaB and p53. Mol Cell Biol. 1999 May;19(5):3485–95.

57. Tergaonkar V, Pando M, Vafa O, Wahl G, Verma I. p53 stabilization is decreased upon NFkappaB activation: a role for NFkappaB in acquisition of resistance to chemotherapy. Cancer Cell. 2002 Jun;1(5):493–503.

58. Kawauchi K, Araki K, Tobiume K, Tanaka N. p53 regulates glucose metabolism through an IKK-NF-kappaB pathway and inhibits cell transformation. Nat Cell Biol. 2008 May;10(5):611–8.

59. Cooks T, Pateras IS, Tarcic O, Solomon H, Schetter AJ, Wilder S, et al. Mutant

p53 prolongs NF-κB activation and promotes chronic inflammation and inflammation-associated colorectal cancer. Cancer Cell. 2013 May;23(5):634–46.

60. Adams JM, Cory S. The Bcl-2 Protein Family: Arbiters of Cell Survival. Science (80-) [Internet]. 1998 Aug 28;281(5381):1322 LP – 1326. Available from: http://science.sciencemag.org/content/281/5381/1322.abstract

61. Wu M, Lee H, Bellas RE, Schauer SL, Arsura M, Katz D, et al. Inhibition of NF-kappaB/Rel induces apoptosis of murine B cells. EMBO J. 1996 Sep;15(17):4682–90.

62. Grumont RJ, Rourke IJ, Gerondakis S. Rel-dependent induction of A1 transcription is required to protect B cells from antigen receptor ligation-induced apoptosis. Genes Dev. 1999 Feb;13(4):400–11.

63. Lee HH, Dadgostar H, Cheng Q, Shu J, Cheng G. NF-κB-mediated up-regulation of Bcl-x and Bfl-1/A1 is required for CD40 survival signaling in B lymphocytes. Proc Natl Acad Sci [Internet]. 1999 Aug 3;96(16):9136 LP – 9141. Available from: http://www.pnas.org/content/96/16/9136.abstract

64. Wang C-Y, Guttridge DC, Mayo MW, Baldwin AS. NF-κB Induces Expression of the Bcl-2 Homologue A1/Bfl-1 To Preferentially Suppress Chemotherapy-Induced Apoptosis. Mol Cell Biol [Internet]. 1999 Sep 1;19(9):5923 LP – 5929. Available from: http://mcb.asm.org/content/19/9/5923.abstract

65. Zong WX, Edelstein LC, Chen C, Bash J, Gélinas C. The prosurvival Bcl-2 homolog Bfl-1/A1 is a direct transcriptional target of NF-kappaB that blocks TNFalpha-induced apoptosis. Genes Dev [Internet]. 1999 Feb 15;13(4):382–7. Available from: https://pubmed.ncbi.nlm.nih.gov/10049353

66. Beg AA, Sha WC, Bronson RT, Ghosh S, Baltimore D. Embryonic lethality and liver degeneration in mice lacking the RelA component of NF-κB. Nature [Internet]. 1995;376(6536):167–70. Available from: https://doi.org/10.1038/376167a0

67. Miyake K, Mickley L, Litman T, Zhan Z, Robey R, Cristensen B, et al. Molecular Cloning of cDNAs Which Are Highly Overexpressed in Mitoxantrone-resistant Cells. Cancer Res [Internet]. 1999 Jan 1;59(1):8 LP – 13. Available from: http://cancerres.aacrjournals.org/content/59/1/8.abstract

68. Lai GM, Chen YN, Mickley LA, Fojo AT, Bates SE. P-glycoprotein expression and schedule dependence of adriamycin cytotoxicity in human colon carcinoma cell lines. Int J cancer. 1991 Nov;49(5):696–703.

69. Shukla S, Jhamtani R, Dahiya M, Agarwal DR. A novel method to achieve high yield of total RNA from zebrafish for expression studies. Vol. 6, International Journal of Bioassays. 2017. 5383 p.

70. Carmichael J, DeGraff WG, Gazdar AF, Minna JD, Mitchell JB. Evaluation of a Tetrazolium-based Semiautomated Colorimetric Assay: Assessment of Chemosensitivity Testing. Cancer Res [Internet]. 1987 Feb 15;47(4):936 LP – 942. Available from: http://cancerres.aacrjournals.org/content/47/4/936.abstract

71. Bahuguna A, Khan I, Bajpai VK, Chul S. MTT assay to evaluate the cytotoxic potential of a drug. Bangladesh J Pharmacol. 2017 Apr 8;12:8.

72. Patel BA, Abel B, Barbuti AM, Velagapudi UK, Chen Z-S, Ambudkar S V, et al. Comprehensive Synthesis of Amino Acid-Derived Thiazole Peptidomimetic Analogues to Understand the Enigmatic Drug/Substrate-Binding Site of P-

Glycoprotein. J Med Chem. 2018 Feb;61(3):834–64.

73.   Jackson SM, Manolaridis I, Kowal J, Zechner M, Taylor NMI, Bause M, et al. Structural basis of small-molecule inhibition of human multidrug transporter ABCG2. Nat Struct Mol Biol [Internet]. 2018;25(4):333–40. Available from: https://doi.org/10.1038/s41594-018-0049-1

74.   Wu Z-X, Yang Y, Teng Q-X, Wang J-Q, Lei Z-N, Wang J-Q, et al. Tivantinib, A c-Met Inhibitor in Clinical Trials, Is Susceptible to ABCG2-Mediated Drug Resistance. Cancers (Basel) [Internet]. 2020 Jan 12;12(1):186. Available from: https://pubmed.ncbi.nlm.nih.gov/31940916

75.   Narayanan S, Gujarati NA, Wang J-Q, Wu Z-X, Koya J, Cui Q, et al. The Novel Benzamide Derivative, VKNG-2, Restores the Efficacy of Chemotherapeutic Drugs in Colon Cancer Cell Lines by Inhibiting the ABCG2 Transporter. Int J Mol Sci [Internet]. 2021 Feb 28;22(5):2463. Available from: https://pubmed.ncbi.nlm.nih.gov/33671108

76.   Bunting KD. ABC Transporters as Phenotypic Markers and Functional Regulators of Stem Cells. Stem Cells [Internet]. 2002 May 1;20(3):274. Available from: https://doi.org/10.1634/stemcells.20-3-274

77.   MILCZAREK M, ROSIŃSKA S, PSURSKI M, MACIEJEWSKA M, KUTNER A, WIETRZYK J. Combined Colonic Cancer Treatment with Vitamin D Analogs and Irinotecan or Oxaliplatin. Anticancer Res [Internet]. 2013 Feb 1;33(2):433–44. Available from: http://ar.iiarjournals.org/content/33/2/433.abstract

78.   Dai C, Tiwari AK, Wu C-P, Su X-D, Wang S-R, Liu D, et al. Lapatinib (Tykerb, GW572016) reverses multidrug resistance in cancer cells by inhibiting the activity

of ATP-binding cassette subfamily B member 1 and G member 2. Cancer Res [Internet]. 2008 Oct 1;68(19):7905–14. Available from: https://www.ncbi.nlm.nih.gov/pubmed/18829547

79. Wang Y-J, Huang Y, Anreddy N, Zhang G-N, Zhang Y-K, Xie M, et al. Tea nanoparticle, a safe and biocompatible nanocarrier, greatly potentiates the anticancer activity of doxorubicin. Oncotarget [Internet]. 2016 Feb 2;7(5):5877–91. Available from: https://www.ncbi.nlm.nih.gov/pubmed/26716507

80. Galante JM, Mortenson MM, Schlieman MG, Virudachalam S, Bold RJ. Targeting NF-kB/BCL-2 pathway increases apoptotic susceptibility to chemotherapy in pancreatic cancer. J Surg Res [Internet]. 2004;121(2):306–7. Available from: https://www.sciencedirect.com/science/article/pii/S0022480404004044

81. Hampel H, Frankel WL, Martin E, Arnold M, Khanduja K, Kuebler P, et al. Screening for the Lynch syndrome (hereditary nonpolyposis colorectal cancer. N Engl J Med. 352(18):1851–1860.

82. Rougier P, Van Cutsem E, Bajetta E, Niederle N, Possinger K, Labianca R, et al. Randomised trial of irinotecan versus fluorouracil by continuous infusion after fluorouracil failure in patients with metastatic colorectal cancer. Lancet. 352(9138):1407–1412.

83. Glusker P, Recht L, Lane B. Reversible posterior leukoencephalopathy syndrome and bevacizumab. N Engl J Med. 354(9):980–982 980–982.

84. Hurwitz H, Fehrenbacher L, Novotny W, Cartwright T, Hainsworth J, Heim W, et al. Bevacizumab plus irinotecan, fluorouracil, and leucovorin for metastatic colorectal cancer. N Engl J Med. 350(23):2335–2342.

85. Hurwitz HI, Fehrenbacher L, Hainsworth JD, Heim W, Berlin J, Holmgren E, et al. Bevacizumab in combination with fluorouracil and leucovorin: an active regimen for first-line metastatic colorectal cancer. J Clin Oncol. 23(15):3502–3508.

86. Patil SA, Patil R. Recent developments in biological activities of indanones. Eur J Med Chem. 138:182–198.

87. Charrier C, Roche J, Gesson JP, Bertrand P. Antiproliferative activities of a library of hybrids between indanones and HDAC inhibitor SAHA and MS-275 analogues. Bioorg Med Chem Lett. 17(22):6142–6146.

88. Gupta P, Kathawala RJ, Wei L, Wang F, Wang X, Druker BJ, et al. PBA2, a novel inhibitor of imatinib-resistant BCR-ABL T315I mutation in chronic myeloid leukemia. Cancer Lett.

89. Malumbres M, Pevarello P, Barbacid M, Bischoff JR. CDK inhibitors in cancer therapy: what is next? Trends Pharmacol Sci. 29(1):16–21.

90. Arnal I, Wade RH. How does taxol stabilize microtubules? Curr Biol. 5(8):900–908.

91. Hastie SB. Interactions of colchicine with tubulin. Pharmacol Ther. 51(3):377–401.

92. Ngamchuea K, Batchelor-McAuley C, Compton RG. Rapid Method for the Quantification of Reduced and Oxidized Glutathione in Human Plasma and Saliva. Anal Chem. 89(5):2901–2908.

93. Circu ML, Aw TY. Reactive oxygen species, cellular redox systems, and apoptosis. Free Radic Biol Med. 48(6):749–762.

94. Matés JM, Sánchez-Jiménez FM. Role of reactive oxygen species in apoptosis:

implications for cancer therapy. Int J Biochem Cell Biol. 32(2):157–170.

95.   Circu ML, Aw TY. Glutathione and apoptosis. Free Radic Res. 42(8):689–706.

96.   Ghosh S, May MJ, Kopp EB. NF-κB AND REL PROTEINS: Evolutionarily
       Conserved Mediators of Immune Responses. Annu Rev Immunol [Internet]. 1998
       Apr 1;16(1):225–60. Available from:
       https://doi.org/10.1146/annurev.immunol.16.1.225

97.   Aggarwal BB, Takada Y, Shishodia S, Gutierrez AM, Oommen O V, Ichikawa H,
       et al. Nuclear transcription factor NF-kappa B: role in biology and medicine.
       Indian J Exp Biol. 2004 Apr;42(4):341–53.

98.   Hayden MS, Ghosh S. Signaling to NF-kappaB. Genes Dev. 2004
       Sep;18(18):2195–224.

99.   Sen R, Smale ST. Selectivity of the NF-{kappa}B response. Cold Spring Harb
       Perspect Biol. 2010 Apr;2(4):a000257.

100.   Mortenson MM, Schlieman MG, Virudalchalam S, Bold RJ. Overexpression of
       BCL-2 results in activation of the AKT/NF-kB Cell survival pathway. J Surg Res
       [Internet]. 2003;114(2):302. Available from:
       https://www.sciencedirect.com/science/article/pii/S002248040300516X

Vita

Name	Silpa Narayanan
Baccalaureate degree	Bachelor of Science
	Mahatma Gandhi University
	Kerala, India
	Major: Zoology
Date graduated	May, 2007
Master's degree	Master of Science
	University of Madras
	Tamil Nadu, India
	Major: Pharmacology
Date graduated	May, 2010